International Journal of Coal Geology 90-91 (2012) 72–99

Contents lists available at SciVerse ScienceDirect

International Journal of Coal Geology

journal homepage: www.elsevier.com/locate/ijcoalgeo

Petrology, mineralogy, and geochemistry of the Ge-rich coal from the Wulantuga Ge ore deposit, Inner Mongolia, China: New data and genetic implications

Shifeng Dai [a,*], Xibo Wang [a], Vladimir V. Seredin [b], James C. Hower [c], Colin R. Ward [d], Jennifer M.K. O'Keefe [e], Wenhui Huang [f], Tian Li [a], Xiao Li [a], Huidong Liu [a], Weifeng Xue [a], Lixin Zhao [a]

[a] State Key Laboratory of Coal Resources and Safe Mining, China University of Mining and Technology, Beijing 100083, China
[b] Institute of Geology of Ore Deposits, Petrography, Mineralogy, and Geochemistry, Russian Academy of Sciences, Staromonetnyi per. 35, Moscow, 119017 Russia
[c] University of Kentucky Center for Applied Energy Research, 2540 Research Park Drive, Lexington, Kentucky 40511, United States
[d] School of Biological, Earth and Environmental Sciences, University of New South Wales, Sydney, NSW 2052, Australia
[e] Department of Earth and Space Sciences, Morehead State University, Morehead, KY 40351, United States
[f] China University of Geosciences, Beijing 100083, China

ARTICLE INFO

Article history:
Received 14 August 2011
Received in revised form 21 October 2011
Accepted 21 October 2011
Available online 28 October 2011

Keywords:
China
Germanium
Lignite
Wulantuga deposit

ABSTRACT

The Early Cretaceous Wulantuga high-Ge coal deposit in Inner Mongolia is one of the major coal-hosted Ge deposits in China. This paper reports new data on the petrological, mineralogical, and geochemical compositions of 13 bench samples of the high-Ge No. 6 coal from the Wulantuga deposit, and provides new insight into the origin and modes of occurrence of the minerals and elements present.

The No. 6 Coal has a low rank ($R_{o,max}$ = 0.45%) and is a low-ash coal (8.77%). The total content of inertinite (52.5 vol.% on average) in most coal benches is higher than that of huminite (46.8 vol.% on average). The dominant huminite maceral is textinite (averages 43.9%), and the dominant inertinite macerals are mainly fusinite (averages 33%) and semifusinite (12.5%), along with trace portions of intertodetrinite, secretinite, funginite, and macrinite. Fungus, seen as the maceral funginite, played a role in the development of degraded maceral forms in the Wulantuga coals. Funginite is present in samples examined in this study, but is not easily extracted during palynological studies; recovered fungal taxa are saprophytes, indicating woody decomposition prior to incorporation in the mire. Palynology revealed a sparse flora that is consistent with the early Cretaceous age.

Minerals in the coal include quartz, kaolinite, illite (and/or illite/smectite), gypsum, pyrite, and traces of rutile and anatase. A varying proportion of bassanite was observed in the low-temperature ashes (LTAs). Bassanite in the LTAs was derived both from the dehydration of gypsum in the raw coals and from the interaction between organically-associated Ca and S during the low-temperature ashing. In addition to a proportion of detrital quartz, fine-grained and cell-filling quartz of authigenic origin is also present. Pyrite is of syngenetic origin and derived from sulfate-rich hydrothermal fluids.

Compared to common Chinese and world low-rank coals, the No. 6 Coal is enriched in Be (25.7 μg/g), F (336 μg/g), Ge (274 μg/g), As (499 μg/g), Sb (240 μg/g), Cs (5.29 μg/g), W (115 μg/g), Hg (3.165 μg/g), and Tl (3.15 μg/g). Germanium in the coal is organically associated, and its enrichment is attributed to hydrothermal fluids from the adjacent granitoids. Beryllium is probably associated with Ca- and Mn-bearing carbonate minerals and to a lesser extent with clay minerals, rather than with organic matter. Fluorine largely occurs in clay minerals (kaolinite and illite). The elevated concentrations of Tl, Hg, As, and Sb are mainly distributed in pyrite and were derived from the same hydrothermal source. The high W in the coal occurs in both the organic matter and the authigenic quartz. Illite is the major carrier of Cs in the coal.

The accumulation of rare earth elements (REE) in the coals had a polygenetic and multistage nature, including two syngenetic stages (early hydrothermal and terrigenous) and one diagenetic (late hydrothermal) stage. The REE distribution patterns of the early hydrothermal and terrigenous stages were characterized by the enrichment of medium REE (M-type REE) and light REE (L-type REE), respectively. A H-type REE distribution pattern (HREE enrichment) occurred in the late diagenetic hydrothermal stage.

The high-Ge Wulantuga coals are also abnormally enriched in precious metals. Gold, Pt, and Pd in the coals, calculated from their concentrations in the LTAs, are 3.5–25.8, < 4–25.5, and < 2.5–15.5 times higher in comparison with those in the continental crust. The highest concentrations of precious metals occur in

* Corresponding author. Tel./fax: +86 10 62341868.

0166-5162/$ – see front matter
doi:10.1016/j.coal.2011.10.012

the pyrite contained in the coal and are 18 (Pd), 130 (Au), and 725 (Pt) times higher than those of the continental crust. The pyrite is probably the basic carrier of the Pt and some portion of the Au in the coal; additionally, a portion of precious metals may be organically (halogen-organic) bound in the coal.

1. Introduction

Under specific geological conditions, some rare and/or noble metals can be significantly enriched in coals, reaching levels equal to or even higher than their concentrations in many conventional types of ores. Although coals with such high trace element concentrations are not common and generally small in volume, these metals could be useful economic by-products of coal cleaning or combustion residues (Dai et al., 2011a; Finkelman and Brown, 1991; Seredin, 2004; Seredin and Dai, in press; Seredin and Shpirt, 1995). For example, Ge from coals is currently being industrially used as raw material (Seredin and Finkelman, 2008). Elements such as Ga, Nb, Zr, Ag, Au, U, REEs (rare earth elements), and PGEs (platinum group elements) have the best chance for such use (Dai et al., 2011a; Seredin and Finkelman, 2008). However, it is unlikely that coal will be an important source of Cu, Zn, Pb, Co, Ni, Cr, As, and Sn in the foreseeable future, not only in China but also in the world, as sufficient conventional ore deposits exist (Dai et al., 2011a; Seredin and Finkelman, 2008).

Studies on Ge in Chinese coals can be traced back to the late 1950s. The reported large coal-hosted Ge deposits in China mainly occur in Lincang (Yunnan), Wulantuga (Inner Mongolia), Yimin (Inner Mongolia) (Du et al., 2003; Hu et al., 2006, 2009; Huang et al., 2008; Li et al., 2011; Qi et al., 2004; 2007a,b; Qing, 2001; Wang, 1999; Zhuang et al., 1998, 2006; Fig. 1), and some small coal basins in southwestern Yunnan province (personal communication with Jianhua Jiang). However, Ge in coals only from Lincang and Wulantuga is being used industrially in China, and the Wulantuga deposit is the largest coal-hosted Ge deposit currently mined in the world.

The Early Cretaceous Wulantuga high-Ge (>100 μg/g) coal deposit is located in the Shengli Coalfield, Inner Mongolia, northeastern China (Fig. 1). Du et al. (2009) estimated that 1700 t of metallic Ge could be extracted from this coal. The origin and modes of occurrence of Ge in the coal have been previously described by Du et al. (2003, 2004, 2009), Li et al. (2011), Qi et al. (2007a,b), Wang (1999), and Zhuang et al. (2006). In this paper, we report new data on the palynological assemblage, maceral composition, mineral origin, and mineralization of associated elements (including Be, F, As, Sb, Cs, Hg, Tl, W, Au, REE, and PGEs) in the coal of the Wulantuga Ge ore deposit.

2. Geological setting

The Shengli Coalfield was deposited in the fault-controlled Shengli sub-basin of the Erlian Basin in northeastern Inner Mongolia (Cui and Li, 1991, 1993). Sub-basins are characterized by thick coal deposits with relatively small areal extent; the Shengli coalfield is 45 km long and 7.6 km wide, with a total area of 342 km^2 (Fig. 1). The Wulantuga Ge deposit only covers an area of 2.2 km^2 within this coalfield, as outlined by the Coal Geology Bureau of Inner Mongolia following two periods of geologic exploration in 1998 and 2005 (Du et al., 2009).

The sedimentary sequences in the Shengli Coalfield include Silurian, Devonian, Permian, Late Jurassic, Early Cretaceous, Neogene, and Quaternary strata (Fig. 2). The Silurian and Devonian strata, with an average thickness of >2363 m, consist of sericite-quartz schist, biotite-quartz schist, two-mica quartz schist, and quartzite.

The Permian sequence has a thickness of 680 – 3550 m. Its upper portion is mainly composed of sandy mudstone, conglomerate, limestone, and siltstone intercalated with limestone layers and lenses of andesitic tuff. The lower portion is made up of bioclastic rocks, marl, limestone, sandstone, and andesite intercalated with andesitic tuff, rhyolite, volcaniclastic rocks, sandstone, mudstone, and conglomerate.

The thickness of the upper Jurassic sequence is greater than 3734 m. It mainly consists of mafic and intermediate-felsic volcanic

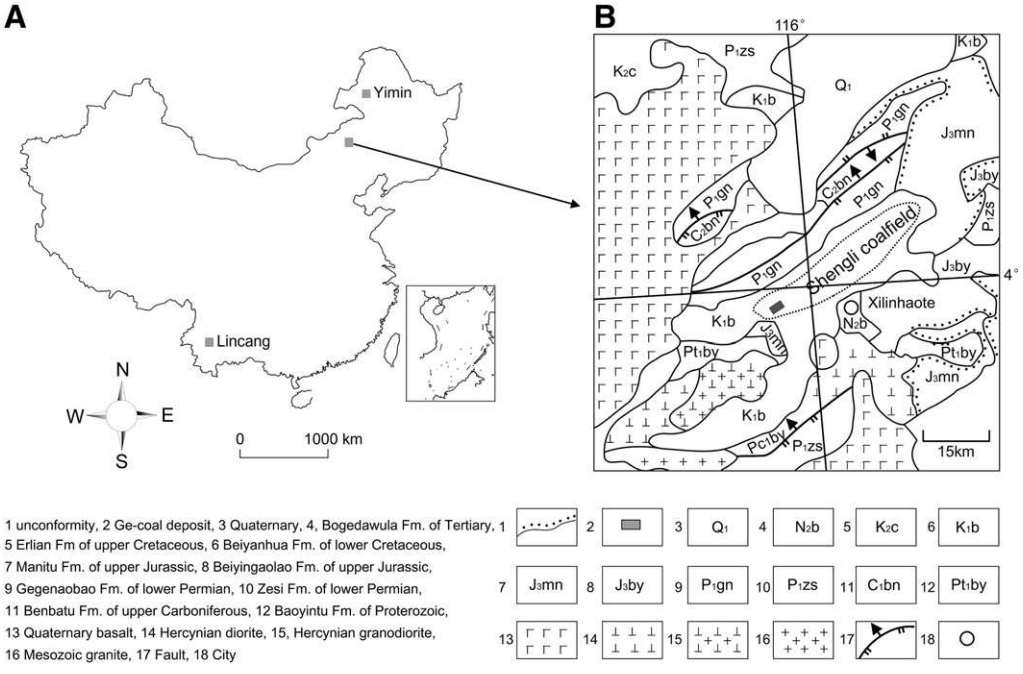

Fig. 1. Location of the Ge ore deposits in China (A) and geological setting of the Wulantuga Ge ore deposit (B; from Wang, 1999, and Du et al., 2009).

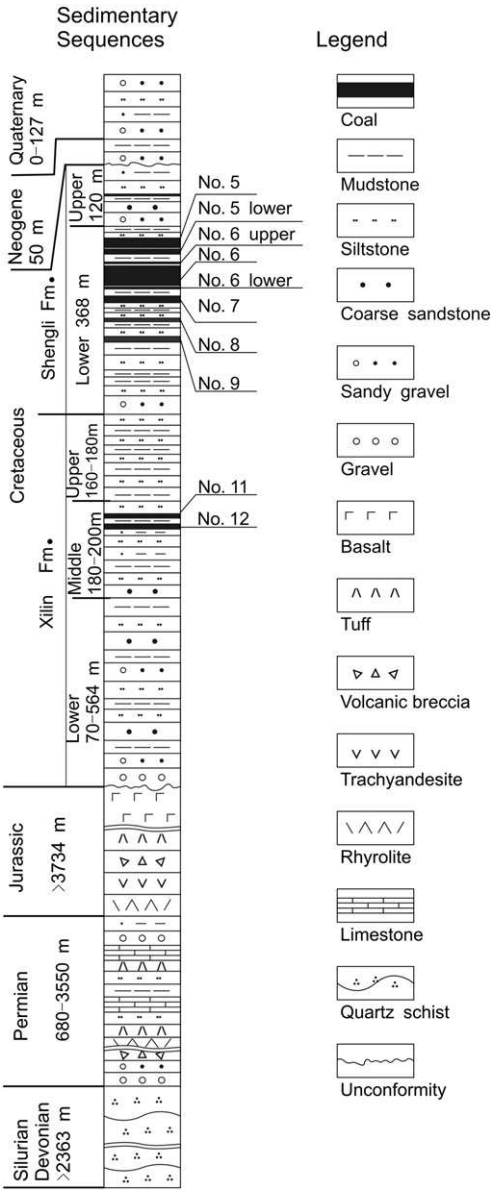

Fig. 2. Sedimentary sequence of the Wulantuga Ge ore deposit (compiled from various geological reports).

rocks, including basalts, tuffs, volcanic breccia, quartz trachyandesite, trachyandesite, and rhyolite.

The coal-bearing lower Cretaceous sequence, collectively called the Bayanhua Group, has a disconformable contact with the underlying Jurassic system, and the underlying Xing'anling Group found elsewhere in the Erlian Basin appears to be absent in this area. The Bayanhua Group was thought to contain four members (Cui and Li, 1991, 1993), but is now generally accepted to include three formations: the Aershan, the Saihantala, and the Hadatu Formations (Sha, 2007). In the Ge-bearing portion of the Shengli Coalfield, the Aershan Formation is called the Tenggeer Group (Qi et al., 2007a) or Xilin Formation, and the Saihantala Formation is called the Shengli Formation. The latter names are used in this work. The Hadatu Formation is absent in the study area. The lower portion (70 – 564 m) of the Xilin Formation is made up of conglomerate and granule gravels interbeded with thin layers of mudstone, fine sandstone, and sandstone. The middle portion (120.43-310.58 m, mostly 180–200 m) of the Xilin Formation is composed of grey mudstone, siltstone, coarse sandstone, and coal beds. The upper portion (132.9-466 m, mostly 160–180 m) of the Xilin Formation is dominated by mudstone and siltstone. There are two coal beds in the Xilin Formation, the Nos. 11 and 12, with average thicknesses of 1.54 m and 2.30 m, respectively.

The lower portion of the Shengli Formation is the major coal-bearing interval, with an average thickness of 368 m; it is mainly made up of coal beds, mudstone, siltstone, fine sandstone, coarse sandstone, and conglomerate. The upper portion (with an average thickness of 120.92 m) is dominated by green-granule gravels intercalated with siltstone and thin layers of coal. There are eight coal beds in the Shengli Formation: Nos. 5 (14.96 m on average), 5-lower (2.98 m on average), 6-upper (unmineable), 6, 6-lower (1.40 m on average), 7 (4.57 m on average), 8 (1.47 m on average), and 9 (1.33 m on average). The No. 6 Coal is the major coal bed with an average thickness of 16.1 m (ranging from 0.8 to 36.2 m).

The Neogene sequence, with an average thickness of 49.84 m, disconformably overlies the Shengli Formation and is composed mainly of gravels and clay.

The Quaternary sequence is up to 127 m thick and consists of sandy soil and gravels.

Tectonically, the Ge deposit is located within a monocline structure with a NW dip and is limited by normal faults on the northeastern and southwestern boundaries (Wang, 1999). The coal seams extend NW from the eroded southeastern outcrop of the deposit across a north-dipping structure. The structural conditions allow the Wulantuga deposit to be worked as a surface mine. The deposit is surrounded on the northwest by Quaternary basalts, on the southwest by Hercynian granodiorite, and on the southeast by Hercynian diorite (Fig. 1).

Table 1
Proximate and ultimate analyses (%), forms of sulfur (%), gross calorific values (GCV, MJ/kg), and maximum huminite reflectance (%) of the No. 6. Coal from the Wulantuga Ore Deposit.

Sample No.	Thickness (cm)	M_{ad}	A_d	V_{daf}	$S_{t,d}$	$S_{s,d}$	$S_{p,d}$	$S_{o,d}$	GCV	C_{daf}	H_{daf}	N_{daf}	$R_{o,max}$
C6-13	100	7.43	8.03	37.22	2.17	0.75	0.61	0.82	24.20	71.25	3.73	0.99	0.47
C6-12	60	6.75	8.94	36.10	1.54	0.26	0.52	0.76	24.22	72.84	4.13	1.00	0.44
C6-11	75	7.38	5.47	36.19	2.08	0.28	1.04	0.75	24.83	72.78	4.05	1.00	0.47
C6-10	60	7.62	6.75	33.27	1.69	0.15	1.05	0.49	25.31	75.55	3.68	1.02	np
C6-9	100	10.34	12.10	34.22	1.88	0.28	0.92	0.67	23.30	76.62	4.06	1.20	0.48
C6-8	100	8.28	8.70	36.52	2.11	0.16	1.02	0.93	24.51	74.49	4.20	1.15	0.45
C6-7	15	9.16	15.90	35.31	1.17	0.12	0.35	0.71	21.69	73.95	4.00	1.06	0.46
C6-6	70	9.89	7.13	34.32	1.07	0.04	0.31	0.71	24.20	76.34	3.82	1.14	0.45
C6-5	50	9.91	7.11	34.30	1.11	0.11	0.34	0.67	24.48	76.08	3.90	1.15	0.42
C6-4	80	8.88	6.48	37.46	2.21	0.48	0.87	0.86	23.85	71.73	4.14	1.02	0.43
C6-3	20	13.57	2.88	42.99	1.41	0.19	0.38	0.84	23.68	73.12	4.16	1.25	0.42
C6-2	40	10.38	8.88	40.18	2.4	0.36	1.04	1.00	23.09	71.43	4.48	1.07	0.44
C6-1	50	11.47	18.60	39.99	2.14	0.38	0.96	0.79	20.55	73.11	4.68	1.52	0.47
WA	820[a]	8.92	8.77	36.32	1.86	0.31	0.78	0.77	23.92	73.86	4.05	1.11	0.45

M, moisture; A, ash yield; V, volatile matter; S_t, total sulfur; S_s, sulfate sulfur; S_p, pyritic sulfur; S_o, organic sulfur; GCV, gross calorific value (air-dry basis); C, carbon; H, hydrogen; N, nitrogen; ad, air-dry basis; d, dry basis; daf, dry and ash-free basis; $R_{o,max}$, maximum huminite reflectance; WA, weighted average; np, not performed; [a], cumulative thickness.

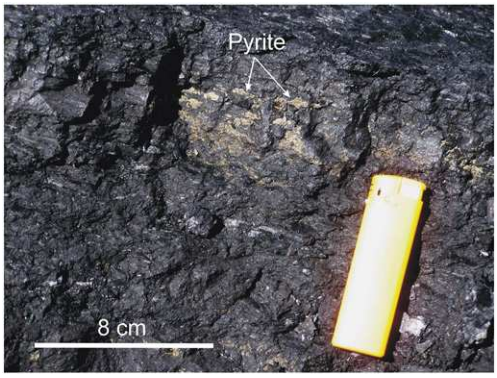

Fig. 3. Pyrite sample collected from the thin intra-seam layer with concretion structure in the lower portion of the seam, close to site of coal seam sampling.

3. Samples and analytical procedures

A total of 13 bench samples were taken from the face of the mined No. 6 coal at the Wulantuga Ge ore deposit in the Shengli Coalfield, following Chinese Standard Method GB/T 482–2008 (2008). Each coal bench sample was cut over an area about 10-cm wide and 10-cm deep. All collected samples were immediately stored in plastic bags to minimize contamination and oxidation. Sample number and thickness are shown in Table 1. From bottom to top, the 13 bench samples of coal are identified as C6-1 to C6-13. The cumulative thickness of the coal in this section is 820 cm, with two partings (10 and 3 cm, respectively) interbedded between the C6-6 & C6-7 and C6-12 & C6-13 bench samples.

Proximate analysis was conducted following ASTM Standards D3173-03 (2005), D3175-02 (2005), and D3174-04 (2005). The total sulfur was determined following ASTM Standards D3177-02 (2005). An elemental analyzer (vario MACRO) was used to determine the percentages of C, H, and N in the coal. Samples were prepared for microscopic analysis in reflected light following ASTM Standard D2797-04 (2005). Maximum reflectance of vitrinite (percent Ro, max) was determined according to ASTM D2798-05 (2005), using a Leitz Orthoplan microscope (at a magnification of 500X) equipped with a Daytronic mainframe 9005 spectrophotometer.

Palynological analysis was conducted following the O'Keefe technique (O'Keefe and Eble, in review; O'Keefe, 2008 [chapter 5 and appendix 6]). Slides were examined using a Leica DM microscope (at a magnification of 500X) equipped with a Spot Pursuit digital camera and a Nikon Labophot2-Pol transmitted light microscope equipped with a Nikon Digital Sight DS-SM camera and interface. Residues were not statistically valid due to poor recovery; therefore, every non-tracer grain present on each slide was examined. Identifications were made using published images and descriptions in Li and Liu (1994), Li and Batten (2004), and Nichols et al. (2006).

The mineralogy was determined by optical microscopic observation and powder X-ray diffraction (XRD). Low-temperature ashing of coal was performed on an EMITECH K1050X plasma asher. The temperature for low-temperature ashing was lower than 200 °C (75 watts power). It took about 12 hours for each one gram sample to be low-temperature ashed.

XRD analysis of the low-temperature ashes and raw coal samples was performed on a D/max-2500/PC powder diffractometer with Ni-filtered Cu-Kα radiation and a scintillation detector. The XRD pattern was recorded over a 2θ interval of 2.6 - 70°, with a step size of 0.01°. X-ray diffractograms of 13 LTA samples and 13 whole-coal samples were subjected to quantitative mineralogical analysis using Siroquant™, commercial interpretation software developed by Taylor (1991) based on the principles for diffractogram profiling set out by Rietveld (1969). Further details indicating the use of this technique for both types of materials are given by Ward et al. (2001).

A scanning electron microscope (Hitachi S-3400 N, 20 kV accelerating voltage) in conjunction with an energy-dispersive X-ray spectrometer (SEM–EDX) was used to study the characteristics of the minerals, and also to determine the distribution of some elements in the coal.

Samples were crushed and ground to pass the 200-mesh sieve for geochemical analysis.

X-ray fluorescence spectrometry (ARL ADVANT'XP+) was used to determine the oxides of major elements for each coal ash (815 °C), including SiO_2, Al_2O_3, CaO, K_2O, Na_2O, Fe_2O_3, MnO, MgO, TiO_2, and P_2O_5. For XRF analysis, the coal ash samples were prepared by borate fusion in an automated fusion furnace (CLAISSE TheBee-10). Each ash sample (1 g) was mixed and homogenized with lithium borate flux (10 g; CLAISSE, pure, 50% $Li_2B_4O_7$ + 50% $LiBO_2$). The mixture was melted in a Pt-Au crucible (25 ml; 95% Pt + 5% Au) and after fusion the melt was cast to a Pt-Au mould flat disk (diameter: 35 mm).

Inductively coupled plasma mass spectrometry (X series II ICP-MS), in a pulse counting mode (three points per peak), was used to determine trace elements in coal samples, except for Hg, F, and Cl. The ICP-MS analysis and sample microwave digestion program, related to coal and coal-related materials, were outlined by Dai et al. (2011b). Arsenic and Se were determined by ICP-MS using collision cell technology (CCT) in order to avoid disturbance of polyatomic ions. For ICP-MS analysis, samples were digested using an UltraClave Microwave High Pressure Reactor (Milestone). The basic load for the digestion tank was composed of 330 ml Mili-Q H_2O, 30 ml 30% H_2O_2 (Metal-Oxide-Semiconductor, MOS reagent), and 2 ml 98% H_2SO_4 (Guaranteed reagent, GR) (Dai et al., 2011b). Initial

Table 2
Maceral composition of the coal from the Wulantuga Ge Ore Deposit (vol.%; on mineral-free basis).

Sample No.	Tex	Ulm	Corp	T-Hum	Fu	Semi	Mac	Sec	Fun	Iner	T-Iner	Spor	Cut	Res	Sub	T-Lipt
C6-13	37.1	2.3		39.4	49.8	4.8	0.4	0.2	1.3	3.8	60.2	0.2			0.2	0.4
C6-12	35.0	1.9		36.9	46.4	6.4		0.8	1.7	7.0	62.3	0.8				0.8
C6-11	40.6	1.7		42.2	33.4	7.4	0.2	3.6	5.0	6.9	56.6	1.2				1.2
C6-10	51.5	0.4		51.9	30.6	11.8	0.2	0.8	0.4	3.4	47.3	0.8				0.8
C6-9	52.2	1.1		53.3	25.5	13.7		1.1	0.4	4.4	45.1	1.7				1.7
C6-8	58.2	1.9		60.1	23.5	10.3		1.4	1.6	3.1	39.9					0.1
C6-7	36.2	1.2		37.4	45.1	12.6		1.2		3.5	62.4	0.2				0.2
C6-6	36.5	1.5		37.9	34.4	21.0		1.3	0.6	4.8	62.1					0.1
C6-5	31.1	1.9		33.1	33.6	25.3		0.5	0.2	6.8	66.4	0.5				0.5
C6-4	34.3	1.9		36.3	36.5	19.7	0.2	1.5	0.6	4.9	63.5	0.2				0.2
C6-3	74.4	18.1	0.4	92.9	2.1	1.9		0.4	1.0	0.8	6.2	0.4	0.4			0.8
C6-2	56.0	12.7	1.1	69.8	14.8	10.8		0.6	0.6	3.0	29.8	0.2		0.2		0.4
C6-1	37.3	5.5	0.2	43.0	34.4	15.1	0.2	1.1	1.3	4.4	56.5	0.4				0.4
WA	43.9	2.8	bdl	46.8	33.0	12.5	bdl	1.2	1.3	4.6	52.5	0.5	bdl	bdl	bdl	0.6

Tex, Textinite; Ulm, Ulminite; Corp, Corpohuminite; T-Hum, total huminite; Fu, Fusinite, Semi, Semifusinite; Mac, Macrinite; Sec, Secretinite; Fun, Funginite; Iner, Inertodetrinite; T-Iner, total inertinite; Spor, Sporinite; Cut, Cutinite; Res, Resinite; Sub, Suberinite; WA, weighted average; bdl, below detection limit.

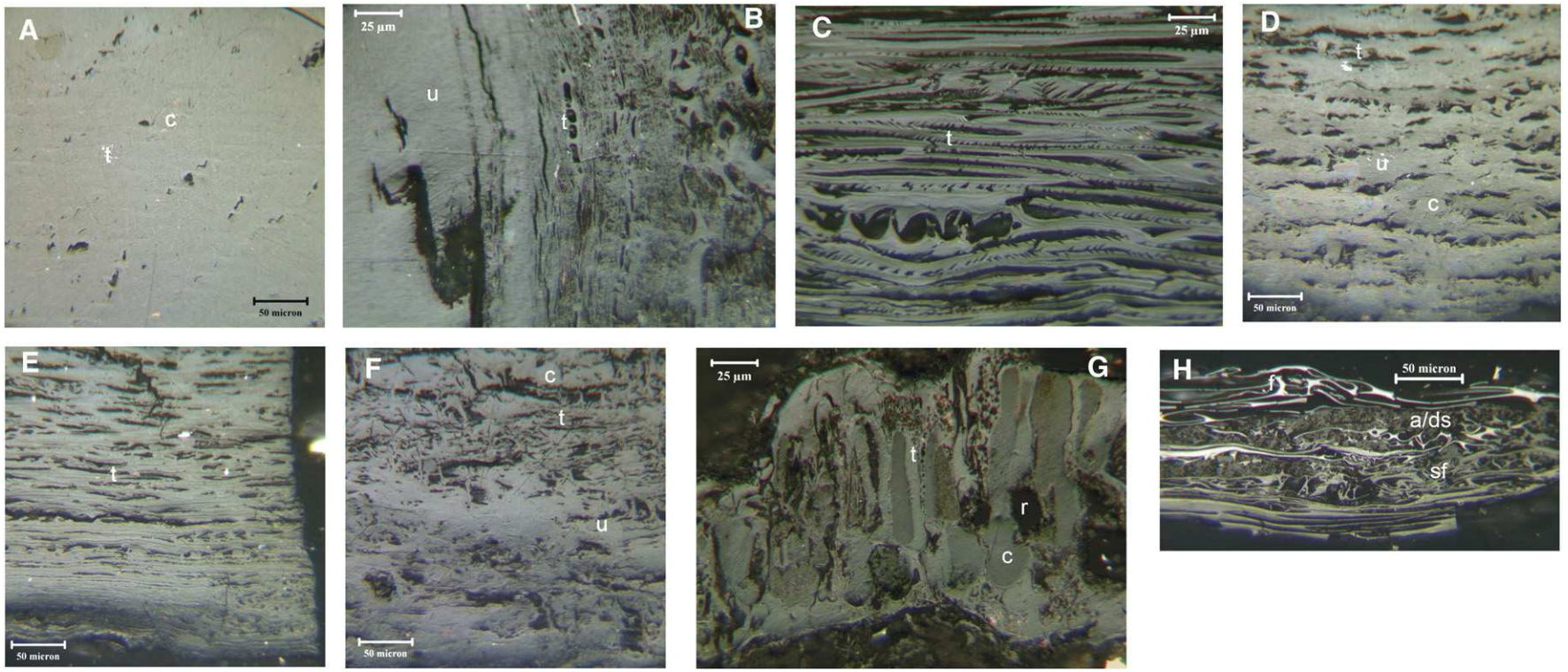

Fig. 4. Taxodiaceae wood showing varying levels of decomposition and gelification. (A) Textinite (t) and corpohuminite (c) (photo 2 01; scale 50 microns). (B) Ulminite (u) and textinite (t) (photo 13 01; scale 25 microns). (C) Textinite (photo 12 04; scale 25 microns). (D) Ulminite (u), textinite (t), and corpohuminite (c) (photo 2 02; scale 50 microns). (E) Textinite (photo 3 10; scale 50 microns). (F) Ulminite (u), textinite (t), and corpohuminite (c) (photo 8 03; scale 50 microns). (G) Resinite (r), textinite (t), and corpohuminite (c) (photo 1 05; scale 25 microns). (H) Fusinite (f) and semifusinite (sf) surrounding attrinite/densinite (a/d) (photo 4 08; scale 50 microns). The first number of the photo (before the space) stands for the coal bench number; the second number (after the space) is the photo sequence number in the coal bench.

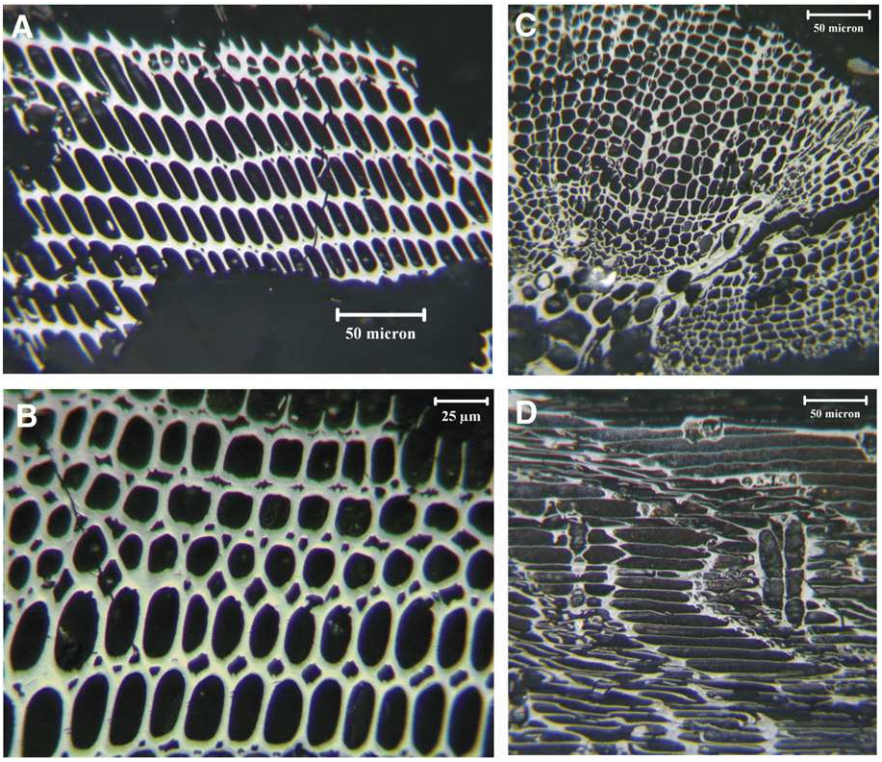

Fig. 5. Fusinite in the coal: (A) photo 5 04, scale 50 microns. (B) photo 10 02, scale 25 microns. (C) burnt fern rachis (photo 9 02; scale 50 microns). (D) Fusinite with clay filling lumens of Taxodiaceae wood (photo 7 03; scale 50 microns).

nitrogen pressure was set at 50 bars and the highest temperature was set at 240 °C for 75 minutes. The reagents digestion of for each 50-mg coal sample were 5 ml 65% HNO_3, 2 ml 40% HF, and 1 ml 30% H_2O_2. The Guaranteed-Reagent HNO_3 and HF for sample digestion were further purified by sub-boiling distillation. Multi-element standards (Inorganic Ventures: CCS-1, CCS-4, CCS-5, and CCS-6) were used for calibration of trace element concentrations.

The concentrations of Au and Pt-group elements were determined for low temperature ashes (<200 °C) derived from three coal bench samples (C6-1, C6-3, and C6-9) and a pyrite sample from a thin (2–3 cm) concretion horizon in the lower portion of the seam close to the sampling site (Fig. 3). For comparison, the concentrations of Au and PGEs were also determined in a high temperature (550 °C) ash sample derived from C6-1. The Au and PGEs determinations were performed in the Institute of Geology of Ore Deposits, Petrography, Mineralogy and Geochemistry, RAS (Moscow). The determination procedure included: (1) Sample chemical digestion using acid decomposition and fusion with sodium peroxide and subsequent transference of the material into hydrochloric acid solution; (2) Sorption concentration of the precious metals from the hydrochloric acid solution by means of organic reagent (Polyorgs IV); (3) Incineration of the reagent and its transference into hydrochloric acid solution; (4) Determination of Pt, Pd, and Au concentration by ICP-MS. The measurements of ^{105}Pd, ^{195}Pt, and ^{197}Au masses were performed also by X Series II ICP-MS. Reference solution "*Multi-element calibration standard 4*" Perkin Elmer Pure Plus 9300234 was used to calibrate the device. The ^{115}In, ^{185}Re, and ^{205}Tl were used as internal standards to prevent device fluctuations. Detection limits, calculated using the method of 3σ-criteria ($n=3$), are Pt 8 ng/g, Au 8 ng/g, and Pd 5 ng/g. The correctness of the method was confirmed by the same analysis of a certified reference material of sulfide copper-nickel ore "SOP 107.1.-04". The method of Au and PGEs determination in the present study was intended to avoid three main analytical problems: (1) The LTA analysis provided an opportunity to estimate the precious metal concentrations in enough representative coal samples with a weight of several grams, and thus can avoid influences of a nugget effect; (2) Using LTAs can avoid the possible loss of volatile Au-PGEs compounds; and (3) pre-concentration and separation of

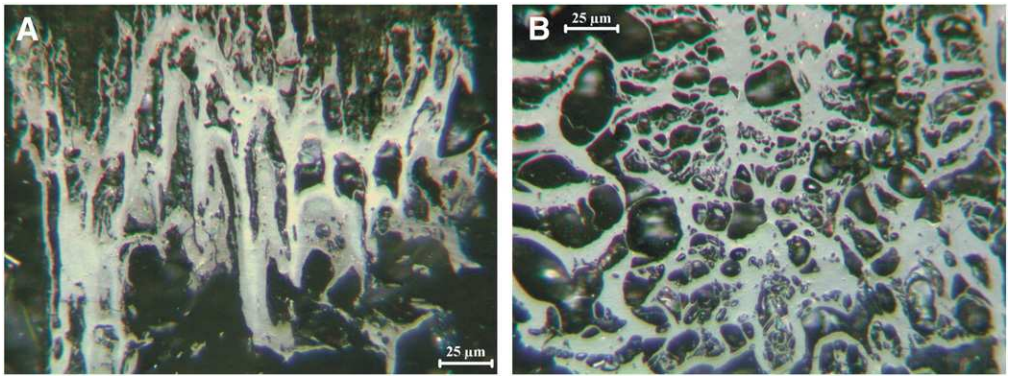

Fig. 6. Degraded fusinite of cell walls prior to oxidation (A) photo 13 03, scale 25 microns. (B) photo 13 04, scale 25 microns.

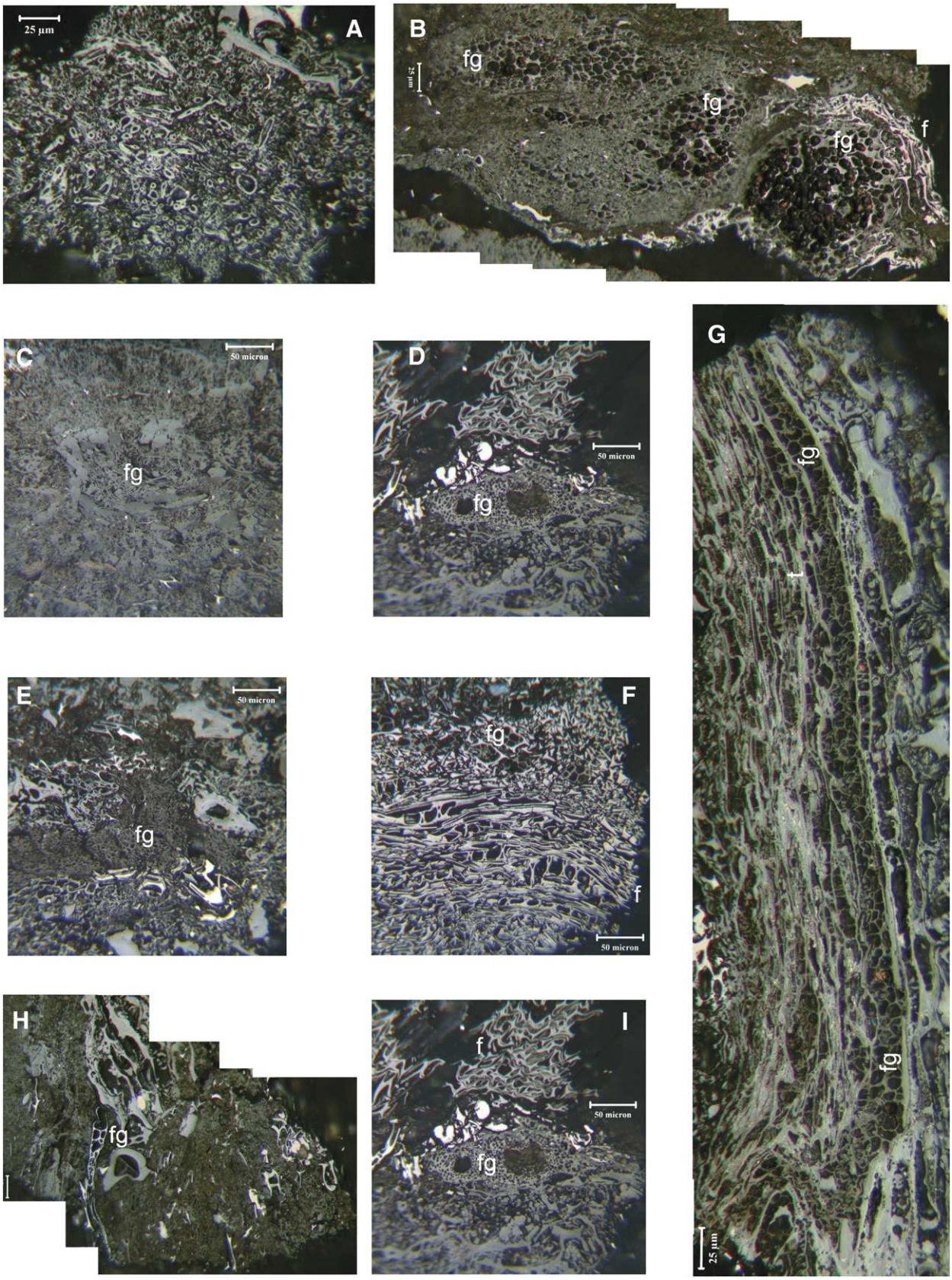

Fig. 7. Funginite in the coal. (A) Fungal hyphae (photo 10 08; scale 25 microns). (B) Funginite (fg) with fusinite (f) (photo 1 01; scale 25 microns). (C) Funginite (fg) as fungal hyphae with cell walls (photo 8 04; scale 50 microns). (D) photo 8 05, scale 50 microns. (E) photo 8 09, scale 50 microns. (F) Funginite (fg) in fusinite (photo 8 12; scale 50 microns). (G) Funginite (fg) in textinite (photo 12 08; scale 25 microns). (H) Fungal hyphae (fg) in attrinite/densinite/porigelinite (?) (photo 12 02; scale 25 microns). (I) Funginite (fg) and macrinite (m) (photo 8 05; scale 50 microns).

the matrix can exclude interference from the analytical lines for other elements that would otherwise not permit the precious metal concentrations to be measured correctly (Qi and Gao, 2008; Seredin, 2007).

Mercury was determined using a Milestone DMA-80 Hg analyzer. Fluorine was determined by pyrohydrolysis with an ion-selective electrode, following the methods described in Chinese Standards GB/T 4633–1997 (1997).

4. Results and discussion

4.1. Proximate and ultimate analyses, huminite reflectance

Table 1 summarizes the results of proximate and ultimate analyses, the forms of sulfur, the gross calorific values, and the mean maximum huminite reflectance data for the 13 coal bench samples from the Wulantuga Ge ore deposit. The averages of mean maximum huminite reflectance, volatile matter (daf: dry and ash-free basis), and gross calorific value (ad: air-dry basis) are 0.45%, 36.32%, and 23.92 MJ/kg, respectively.

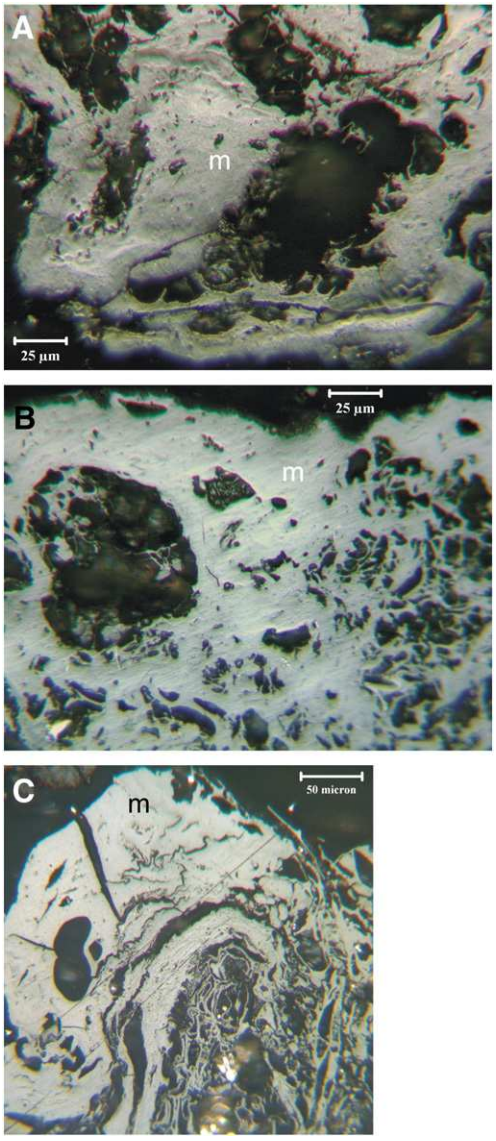

Fig. 8. Macrinite (m) in the coal. (A) photo 1 12, scale 25 microns. (B) photo 10 03, scale 25 microns. (C) photo 4 04, scale 50 microns.

The coal displays high moisture values (averages 8.92%). It is a low-ash and medium- to high-sulfur coal, according to Chinese Standards GB/T 15224.1-2004 (2004a); coals with ash yield <16.00% are low-ash coals) and GB/T 15224.2-2004 (2004b); coals with total sulfur content 1.51-3.00% are medium- to high-sulfur coals). The average contents of pyritic and organic sulfur are 0.78% and 0.77%, respectively (Table 1). Owing to the gypsum in the raw coal samples as described below, the sulfate sulfur is relatively high, averaging 0.31%.

The average ash yield (8.77%) and sulfur content (1.86%) presented in this section are respectively lower and higher than those (21% and 1%, respectively) reported by Zhuang et al. (2006); this indicates significant lateral variations in the ore deposit.

4.2. Maceral composition

The maceral classification and terminology applied in the current study is based on Taylor et al. (1998) and the ICCP System 1994 (ICCP, 2001; Sýkorová et al., 2005).

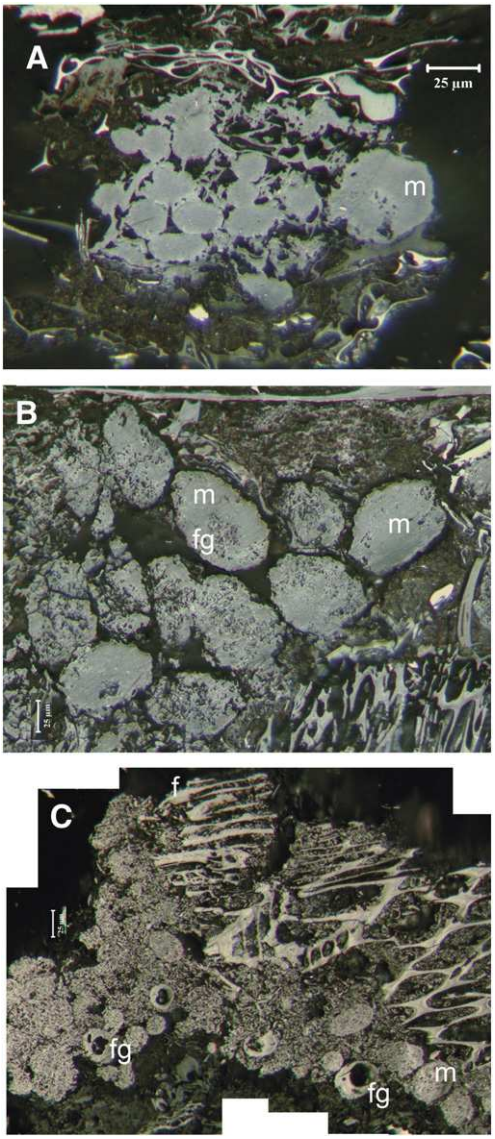

Fig. 9. Macrinite (m) in the coal. (A) Macrinite (m), possibly in the form of coprolites (photo 11 02; scale 25 microns). (B) Macrinite (m) with funginite within macrinite balls (photo 11 03; scale 25 microns). (C) Macrinite (m) with fusinite (f) and poorly indurated inertinitic macerals, possibly after gelinite; fine funginite (fg) also present (photo 1 13; scale 25 microns).

The maceral composition is listed in Table 2. The total content of inertinite in most coal benches is higher than that of total huminite. The weighted averages of the inertinite and huminite contents in the coal bed are 52.5% and 46.8%, respectively. The liptinite content is low, averaging 0.6%.

The dominant huminite maceral is textinite, varying from 31.1% to 58.2%, with a weighted average of 43.9%. A small proportion of ulminite occurs (0.4-12.7%) throughout the section, but corpohuminite could be quantitatively determined only in the lower portion of the seam (C6-1, C6-2, and C6-3). Some of the best development and preservation of huminite macerals is found in forms derived from Taxodiaceous wood (Fig. 4). The examples in Fig. 4A-C show varying, but generally good levels of preservation, with fewer signs of degradation than those seen in Fig. 4D-F. Fig. 4C, in particular, shows well-preserved textinite, in contrast to the poor preservation of the textinite cell walls in Fig. 4D-F. Resinite as cell filling is seen in Fig. 4G. Poorly consolidated huminite macerals, as attrinite and densinite, are common throughout the sample suite (Fig. 4H).

The inertinite macerals are mainly fusinite and semifusinite, along with trace portions of intertodetrinite, secretinite, funginite, and macrinite. However, in sample C6-3, the inertinite content is much lower (only 6.2%). Fusinite (Fig. 5) is also represented by forms indicative of burning of wood and other plant materials, as discussed for other coals (Guo and Bustin, 1998; Scott, 1989, 2000, 2002; Scott and Glasspool, 2005, 2007; Scott and Jones, 1994; Scott et al., 2000). Fusinite also occurs in a degraded form (Fig. 6), suggesting that it was on a path to degradation, possibly to macrinite (Hower et al., 2009, 2011a), before oxidation.

Fungus, seen as the maceral funginite (Fig. 7), is known to play a role in the development of degraded maceral forms (Belkin et al., 2009, 2010; Hower and Ruppert, 2011; Hower et al., 2009, 2010, 2011a,b; O'Keefe and Hower, 2011; and references therein). The development of macrinite, the product of fungal and, probably also, bacterial degradation, can result in the formation of a relatively amorphous form with few, if any, included non-macrinite macerals (Fig. 8). Macrinite can also take on a rounded form (Fig. 9), suggestive of a coprolitic origin (Hower et al., 2011a). Funginite may be included within the macrinite (Fig. 9A, B), suggesting fungal colonization of the coprolite. Macrinite with inclusions of liptinite and fusinite, common in the coals studied by Hower et al. (2009, 2011a), was not observed in the Wulantuga samples.

The liptinite macerals are mainly represented by sporinite and traces of cutinite (Fig. 10A), resinite (Fig. 10B), and suberinite (Fig. 10C-D).

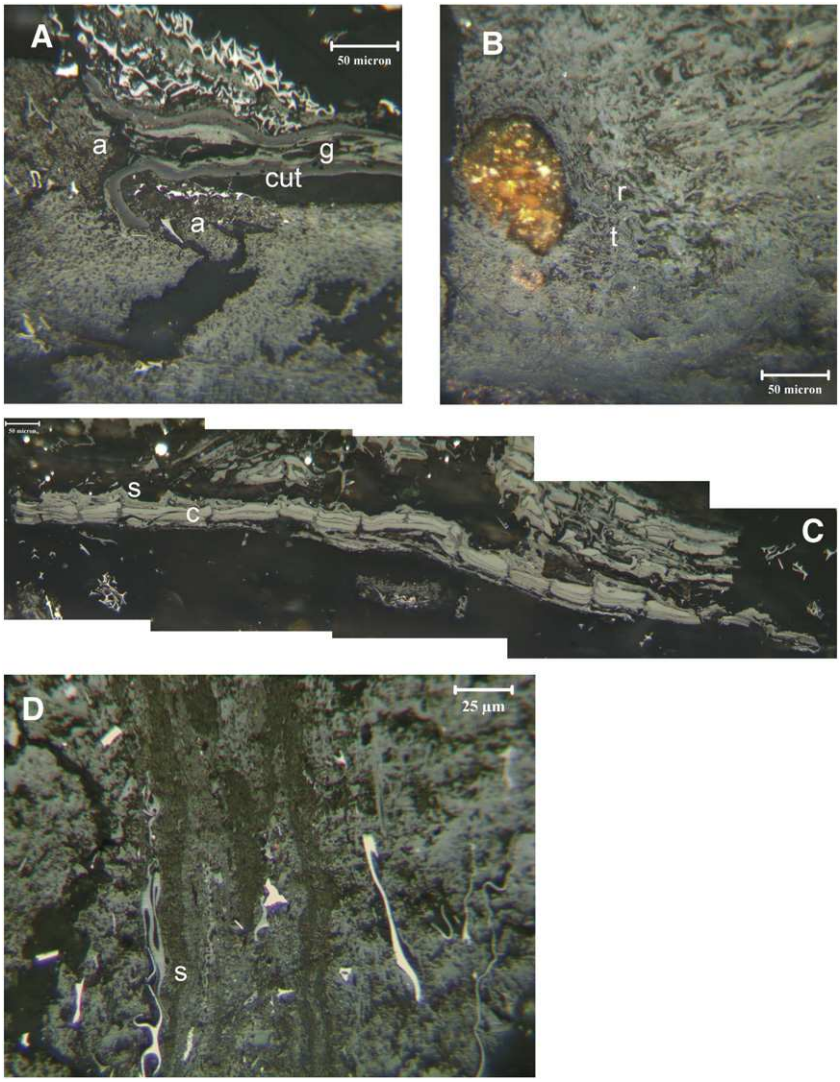

Fig. 10. Liptinite in the coal. (A) Cutinite (cut) with gelinite (g) between leaves. Attrinite/densinite (a), typical of much of the huminite in this coal, is seen below cutinite (photo 4 03; scale 50 microns). (B) Resinite (r) in textinite (t) (photo 3 06; scale 50 microns). (C) Suberinite (s) with corpohuminite (c) cell fillings (photo 1 suberinite; scale 50 microns). (D) Suberinite (s) (photo 12 06; scale 25 microns).

4.3. Sporomorph assemblage

Sporomorph recovery was very low, with tracer lycopodium spores outnumbering authigenic sporomorphs. This appears to have been a function of 1) the overall low sporinite and funginite contents (the coals are fusinite and textinite dominated); 2) the intractability of fusinite (it is both chemically stable and has a density similar to sporopollenin, thus it is retained in the "float" fraction); and 3) the challenge of recovering fungal forms from coals with reflectances higher than 0.4% R_r (O'Keefe et al., 2011).

In all thirteen samples, the assemblage is dominated by bryophytes, pteridophytes, and gymnosperms (Fig. 11). Bryophytes include *Stereisporites stereoides* and *Triporoletes singularis*. Pteridophytes include *Crybelosporites* sp., *Cicatrcosisporites imbricatus*, *Impardecispora cavernosa*, *Lygodiumsporites* sp., *Neoraistrickia* sp., *Osmudacidites* sp., and *Verrucosisporites rotundus*. Gymnosperms include *Cedripites* sp., *Classopollis* sp., *Cycadopites* sp., *Ephedripites* sp., *Inaperturopollenites* sp., *Pityosporites* sp., and *Pristinuspollenites* sp. Fungal forms are present, but rare in the preparations. They include EMA-28 of Prager et al. (2006), *Exesisporites* sp., *Hypoxylonites* sp., a spore of unknown affinity, and fungal hyphae.

The sporomorph spectrum is not identical to spectra obtained elsewhere in the Erlian Basin (Wang and Qian, 1981), although it has similarities to the spectra recovered from this and other basins (Li and Liu, 1994; Wan et al., 2000; Wang and Zhang, 1985; Yang et al., 2007). It is much like the spectrum recovered by Nichols et al. (2006) from the Khuren Dukh Formation in Mongolia; variations are likely due to the different depositional environment, as the samples studied by Nichols et al. (2006) were mudstones. Of note is that no *Asteropollis* sp. pollen was recovered, indicating that this deposit may be somewhat older than the Albian-aged Khuren Dukh Formation. This observation is consistent with the Aptian age cited by Sha (2007). All recovered sporomorphs are consistent with freshwater deposition; no marine or estuarine indicator taxa were recovered.

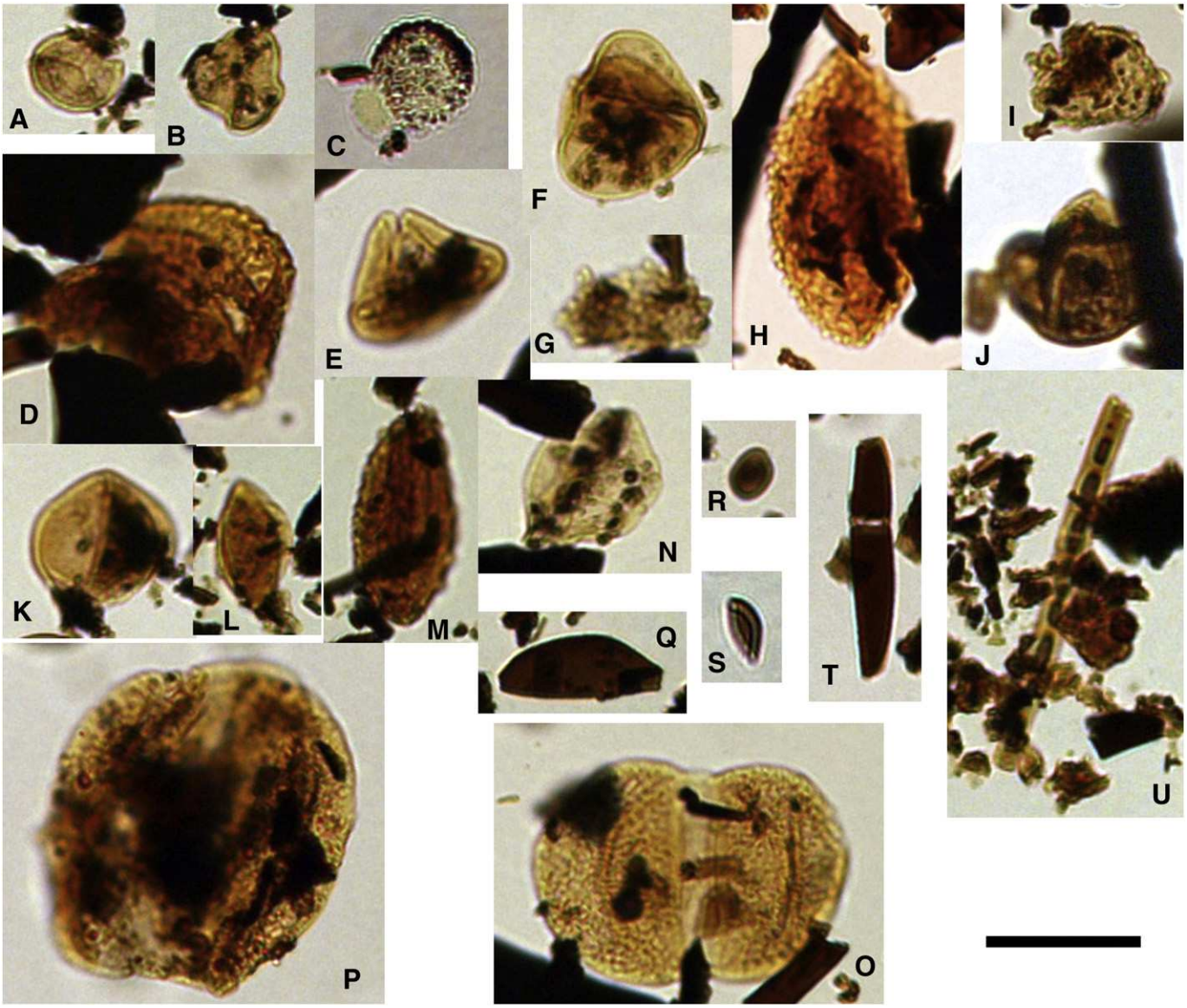

Fig. 11. Sporomorphs recovered from the coal. (A) *Stereisporites stereoides*, (B) *Triporoletes singularis*, (C) *Crybelosporites* sp., (D) *Cicatrcosisporites imbricatus*, (E) *Impardecispora cavernosa*, (F) *Lygodiumsporites* sp., (G) *Neoraistrickia* sp., (H) *Osmudacidites* sp., (I) *Verrucosisporites rotundus*, (J) *Cedripites* sp., (K) Classopollis sp., (L) Cycadopites sp., (M) *Ephedripites* sp., (N) *Inaperturopollenites* sp., (O) *Pityosporites* sp., (P) *Pristinuspollenites* sp., (Q) EMA-28 of Prager et al. (2006), (R) *Exesisporites* sp., (S) *Hypoxylonites* sp., (T) spore of unknown affinity, and (U) an example of fungal hypha. (Scale bar at the bottom right side 25 microns).

Table 3
Mineralogical composition of raw coal (wt. % of crystalline phases) applying X-ray diffraction and Siroquant.

Sample No.	LTA yield (wt.%)	Quartz	Kaolinite	Illite	I/S	Pyrite	Gypsum
C6-13	*10.64*	55.9	7.2			18.8	18.1
C6-12	*11.92*	49.3	28.3	3.9		11.0	7.6
C6-11	*8.47*	26.4	11.8			42.6	19.2
C6-10	*10.15*	35.3	27.6			26.2	10.9
C6-9	*19.87*	13.8	56.5	0.6		10.4	3.6
C6-8	*12.61*	29.4	24.9	19.5		21.5	4.6
C6-7	*21.11*	51.0	35.4	4.8		4.4	4.4
C6-6	*11.09*	41.5	43.8			8.5	6.1
C6-5	*10.39*	38.9	41.0	6.5		8.0	5.7
C6-4	*11.38*	20.4	23.2	19.1		20.8	16.5
C6-3	*8.71*						
C6-2	*13.91*	43.7	20.5	5.3		21.9	8.6
C6-1	*29.53*	30.1	23.4	6.2	22.1	8.0	10.2
WA	13.42	34.33	28.24			18.12	10.17

Note: The high level of organic matter prevented analysis of sample C6-3. WA, weighted average.

4.4. Mineralogical composition

4.4.1. Minerals in whole coal samples

The proportion of each crystalline phase from XRD analysis of the whole-coal samples is listed in Table 3. As discussed by Ward et al. (2001), the high background due to the organic matter was removed from each of the diffractograms as part of the Siroquant processing, and the percentages given in Table 3 reflect the proportion of each phase as a fraction of the total crystalline mineral matter.

Quartz, kaolinite, illite, pyrite, and, in one case, interstratified illite/smectite (I/S) are recognised in the XRD patterns of the whole-coal samples. The proportions of illite and I/S, however, are difficult to determine, due to overlap with the background pattern of the organic matter. Significant proportions of gypsum ($CaSO_4\ 2H_2O$) are also present in the whole-coal samples.

4.4.2. Minerals in LTAs

The proportion of each crystalline phase identified from the diffractograms of the LTA samples is given in Table 4. The phases identified in the LTAs include quartz, kaolinite, illite (and/or illite/smectite), pyrite, rutile, and anatase, as well as a varying proportion of bassanite ($CaSO_4.½H_2O$). A significant proportion of amorphous material is also indicated in the XRD pattern of sample C6-3, and to a lesser extent in some of the other LTA samples. Since the composition and XRD characteristics of any amorphous material are uncertain, it has not been included in Table 4; the data presented for the LTA samples refer only to the crystalline phases determined.

4.4.3. Comparison of whole-coal and LTA samples

The crystalline phases identified in most raw coal bench samples are in accordance with those in the LTAs. A high proportion of gypsum was identified in the raw coals; this mineral is not present in the LTAs, although varying percentages of bassanite were identified in the LTAs.

As discussed further by Frazer and Belcher (1973), Ward (2002), and Ward et al. (2001), the bassanite in the LTA of coal samples is commonly thought to be formed as an artifact of the plasma-ashing process, derived from interaction of organically-associated Ca and sulfur released from the maceral components during oxidation. An exception may occur when sulfuric acid produced by oxidation of pyrite during storage of the coal reacts with calcite (if present) to form gypsum, which is then partly dehydrated during the low-temperature ashing process (Rao and Gluskoter, 1973). However, gypsum may also be present as a crystalline phase in (un-ashed) lower-rank coals (e.g. Koukouzas et al., 2010), either as an authigenic mineral within the coal or as a product of Ca and SO_4 ions precipitated from the pore water during air or oven drying of the coal samples. Such gypsum, if present, would also be partly dehydrated to bassanite by the plasma ashing process.

The presence of gypsum in the raw coal samples of the present study (Table 4) suggests that some of the bassanite in the LTAs, at least, may represent a dehydration product of gypsum contained in the coal samples. In some cases (e.g. C6-4, C6-11, C6-13) the proportion of gypsum is similar to that of bassanite; in other cases, however (e.g. C6-5, C6-7, C6-12), the proportion of bassanite in the LTA is much higher than would be expected if it had all been derived from the gypsum in the respective un-ashed coal samples. For these coals, at least, it appears that much of the bassanite in the LTAs was produced as an artifact from interaction of organically-associated Ca and S during oxidation of the organic matter.

The proportion of LTA for the samples studied is approximately 1.4 times the high-temperature ash yield (Fig. 12A). The difference is partly due to dehydration of the clay minerals, oxidation of the pyrite, and conversion of the gypsum or the bassanite-forming components to either anhydrite or lime during the (high-temperature) ashing process.

The proportion of bassanite in the LTAs shows an overall negative relationship to the LTA yield (Fig. 12B), suggesting an association with the organic matter. With one exception (the high-ash coal of sample C6-1), the proportion of bassanite in the LTA is higher than that of gypsum in the crystalline matter of the raw coal (Fig. 12C). Some samples plot relatively close to the diagonal equality line, suggesting that most of the bassanite in the relevant LTAs was derived from gypsum in the raw coals. Many others, however, plot well above the line, suggesting formation of most of the bassanite in those samples as an artifact of the low-temperature ashing.

Table 4
Mineralogical composition of LTA samples (wt. %) determined applying X-ray diffraction and Siroquant.

Sample No.	LTA yield (wt.%)	Quartz	Kaolinite	Illite	I/S	Pyrite	Rutile	Anatase	Bassanite
C6-13	10.64	48.0	11.2			22.1			18.7
C6-12	11.92	43.8	26.0	7.7		9.9			12.6
C6-11	8.47	23.1	11.9		12.0	26.6			26.4
C6-10	10.15	28.4	34.6	3.8		7.8	0.2		25.2
C6-9	19.87	10.4	53.0	18.0		9.9	0.3	0.7	7.6
C6-8	12.61	27.8	32.1			21.9			18.2
C6-7	21.11	37.6	32.7	9.4		4.8	0.6		14.8
C6-6	11.09	23.4	22.8			24.6	0.6		28.7
C6-5	10.39	28.9	33.7	4.0		8.1	0.3		25.0
C6-4	11.38	19.8	22.8	5.7		25.9			25.8
C6-3*	8.71	22.9	25.6	5.8		27.3			18.5
C6-2	13.91	33.6	22.5	10.9		18.4			14.5
C6-1	29.53	20.5	30.4	41.1		5.5			2.5
WA	13.42	27.73	27.67			17.41			18.68

Note: Asterisk (*) indicates a significant proportion of amorphous material is also present. WA, weighted average.

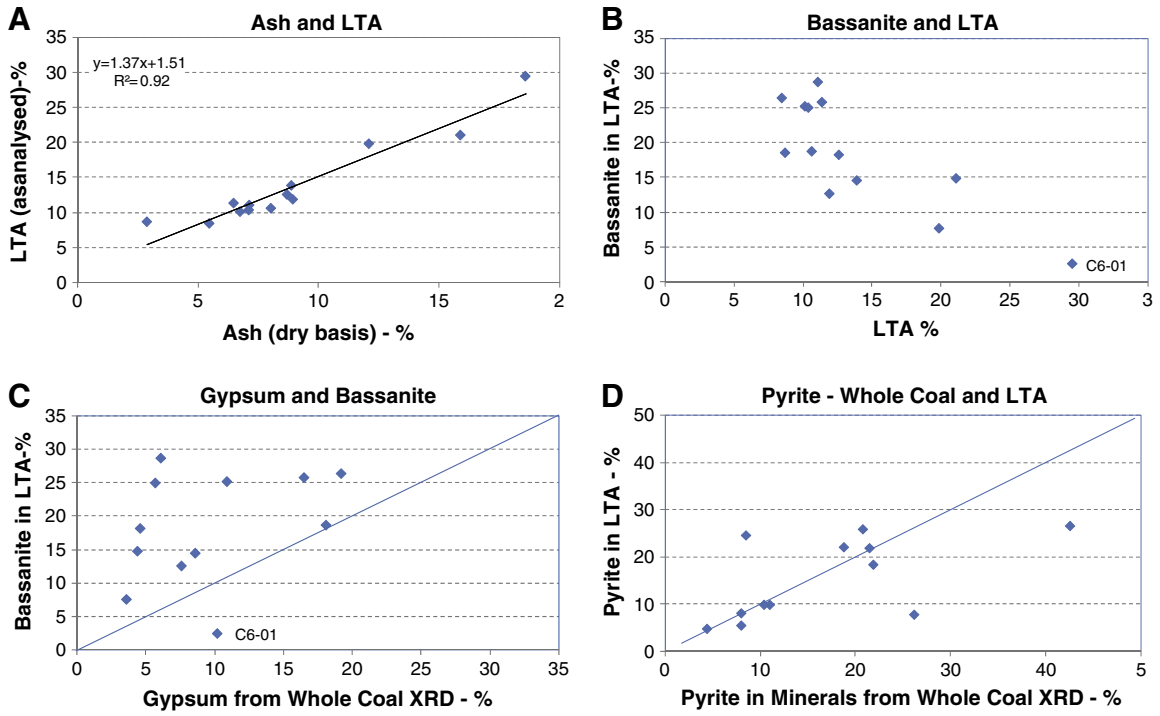

Fig. 12. Relations between selected mineral matter components: (A), High temperature ash vs low temperature ash; (B), bassanite content of LTA vs LTA yield; (C), gypsum in whole-coal vs bassanite in LTA; (D) pyrite in raw coal vs pyrite in LTA.

The proportion of pyrite in the whole coals, expressed as a percentage of the crystalline mineral matter, is very similar for most of the coals to the percentage of pyrite in the LTA of the same coal samples (Fig. 12D). The few exceptions (e.g. C6-6, C6-10, C6-11) may represent cases where segregation occurred during sample splitting or preparation.

Based on XRD analysis for whole-coal samples, Zhuang et al. (2006) and Du et al. (2009) showed that major minerals in the No. 6 Coal are quartz, kaolinite, illite, montmorillonite, clinochlore, gypsum, and pyrite; whereas calcite, dolomite, and feldspar occur in traces. Traces of scheelite ($CaWO_4$) and weddellite (an oxalate, $CaC_2O_4\,2H_2O$) were also detected (Zhuang et al., 2006). A number

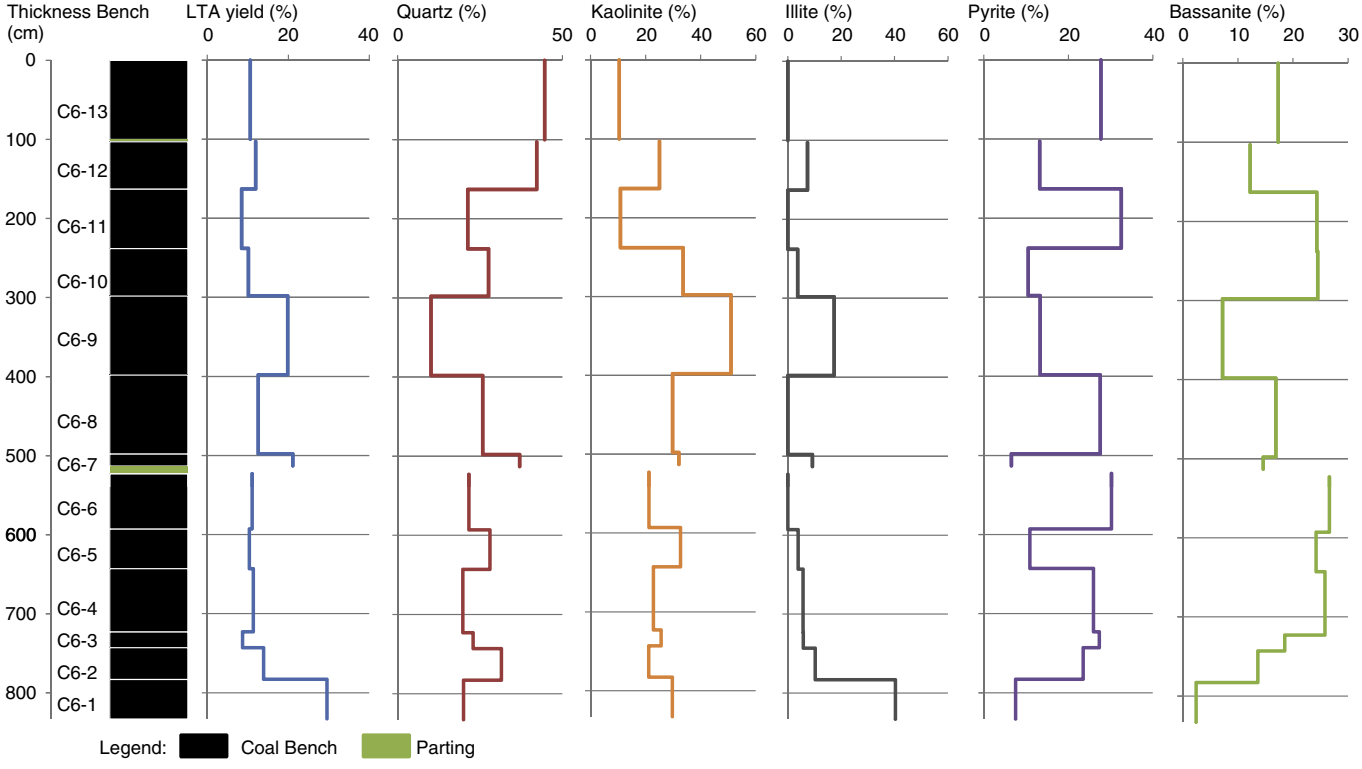

Fig. 13. Low temperature ash yield and the mineral contents along the coal profile studied.

of these minerals, including calcite, dolomite, feldspar, scheelite, and weddellite, were not detected in the section covered by the present study, even though XRD analysis for the present study was performed on both LTAs and raw coal samples.

4.4.4. Quartz

Quartz in the LTAs of the section studied varies from 10.1 to 44.6% with a weighted average of 26.4%. Quartz is enriched in the upper portion of the section and has an inverse variation with LTA yield (Fig. 13). Quartz in the Wulantuga coals was considered by Zhuang et al. (2006) as detrital material of terrigenous origin. However, while a small proportion of the quartz occurs as fragments that are clearly of detrital origin, judged from their subangular shape, large size (>20 μm), and their long axis parallel to bedding (Fig. 14A), the mode of occurrence of most of the quartz is either as cell-fillings (Fig. 14B, C) or as fine-grained particles (generally<5 μm) restricted to the organic matter (Fig. 14B, C), both of which clearly indicate an authigenic precipitation process. It is very difficult to form fine-grained quartz with a size <10 μm during mechanical transport from the sediment-source region to the mire, although the particle size of quartz in coal depends on both the transport distance and the relief energy. Quartz of detrital origin generally has a silt- to sand-size (Kemezys and Taylor, 1964; Ruppert et al., 1991). Ren (1996) has shown that the quartz of detrital origin in many Chinese coals usually has a silt size (0.0625 – 0.0039 mm). Dai et al. (2008) showed that the ultrafine size of quartz (nm to <10 μm) in the Late Permian coals of eastern Yunnan, China, and its modes of cell-filling occurrence indicate that the quartz is of authigenic origin. Fine-grained quartz, thought from its lack of response to cathodoluminescence to be of authigenic origin, is also common in the interior parts of the Upper Freeport coal seam, in areas devoid of more luminescent detrital quartz grains (Ruppert et al., 1985, 1991).

The authigenic quartz in the Wulantuga coals was probably deposited from silica-containing solutions originating from the weathering of granite to the southwest and/or south of the coal basin. The relatively high W in the quartz, as described below, further supports an authigenic precipitation process.

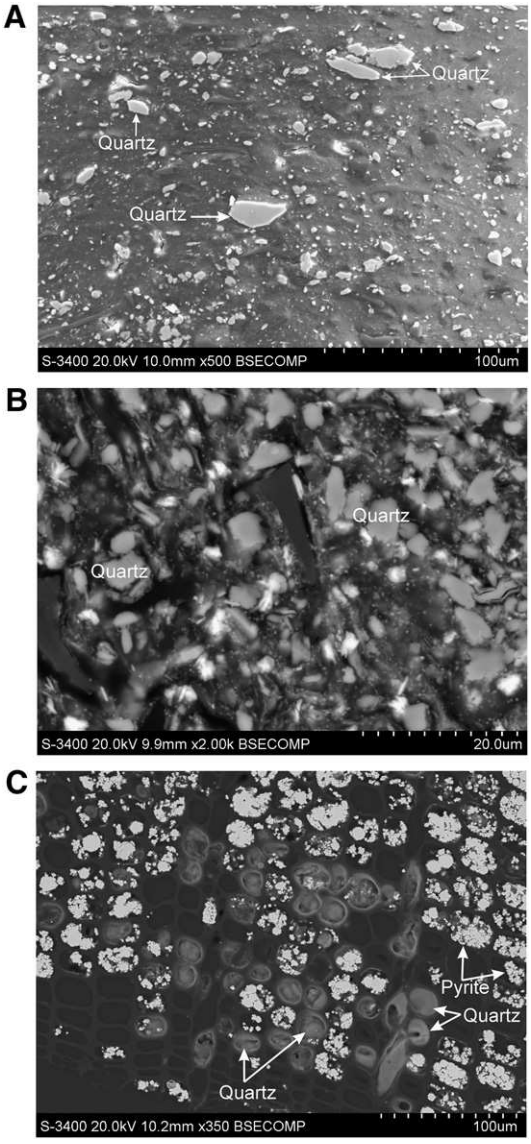

Fig. 14. Quartz and pyrite in the Wulantuga coal. SEM, electron backscattering images. (A), Subangular quartz and fine-grained quartz in collodetrinite; (B), Fine-grained quartz; (C), Cell-filling quartz and pyrite.

4.4.5. Pyrite and clausthalite

Pyrite occurs in each bench sample throughout the entire coal seam section. Its proportion in the LTA varies from 4.8 to 27.3%, with a weighted average of 17.41%. The correlation coefficients of pyrite to LTA, kaolinite, and illite are −0.63, -0.62, and −0.36, respectively. Pyrite has an inverse variation with LTA yield, kaolinite, and illite along the section in the present study (Fig. 13).

Pyrite occurs mainly in cell-filling (Fig. 14C), euhedral (Fig. 15A, B), framboidal (Fig. 15C, overgrown framboids in G), and massive (Fig. 15D-G) forms. The coal formed in a nonmarine environment and was not influenced by seawater during peat accumulation or the post-depositional stage (Han et al., 1996). Generally, sea water favors pyrite formation, and the presence of syngenetic pyrite is often considered as an indicator of marine influence. However, pyrite of syngenetic origin may also be abundant in coals formed in freshwater environments that do not obviously connect to seawater (Ward, 1991), suggesting that sulfate-rich groundwater or hydrothermal fluids may be involved in pyrite formation (Boctor et al., 1976; Kortenski and Kostova, 1996; Siavalas et al., 2009). Considering its depositional environment and modes of occurrence, the pyrite in the Wulantuga coal is of syngenetic origin and was probably derived from hydrothermal fluids.

Clausthalite is a trace mineral in the coals (Fig. 16).

4.4.6. Clay minerals

The crystalline clay mineral phases identified from the diffractograms of the LTA samples include kaolinite and illite (and/or illite/smectite).

Kaolinite is enriched in the middle portion of the seam and is less abundant in the upper portion of the section (Fig. 13). In most of the LTAs, the kaolinite is relatively poorly ordered, whereas in sample C6-9, and to a lesser extent in samples C6-5 and C6-10, it is moderately well ordered. The poorly ordered kaolinite may indicate a detrital origin (Liu and Zhang, 1997; Ward, 2002). A small proportion of epigenetic kaolinite, occurring as fracture-fillings, was observed under SEM-EDX (Fig. 17). The size of the individual particles in the epigenetic kaolinite aggregates is less than 1 μm (Fig. 17).

The illite mostly has a d(001) spacing of around 10.1 Å, suggesting possibly some interlayering with smectite. The LTA of sample C6-11, however, has a broad diffraction peak at around 12 Å, suggesting a more definite illite/smectite (I/S) structure (Fig. 18).

A trace amount of chlorite was detected under SEM-EDX (Fig. 19), but its proportion in both the raw coal samples and the LTAs is below the XRD detection limit. Chlorite is common in coal but often occurs in high-rank coals (Vassilev et al., 1996). Chamosite (Fe-variety) and clinochlore (Mg-variety) are the two common forms of chlorite. SEM-EDX data (Table 5) show that the concentration of Fe and Mg in the chlorite is 15.34% and 6.27%, respectively, indicating a clinochlore variety.

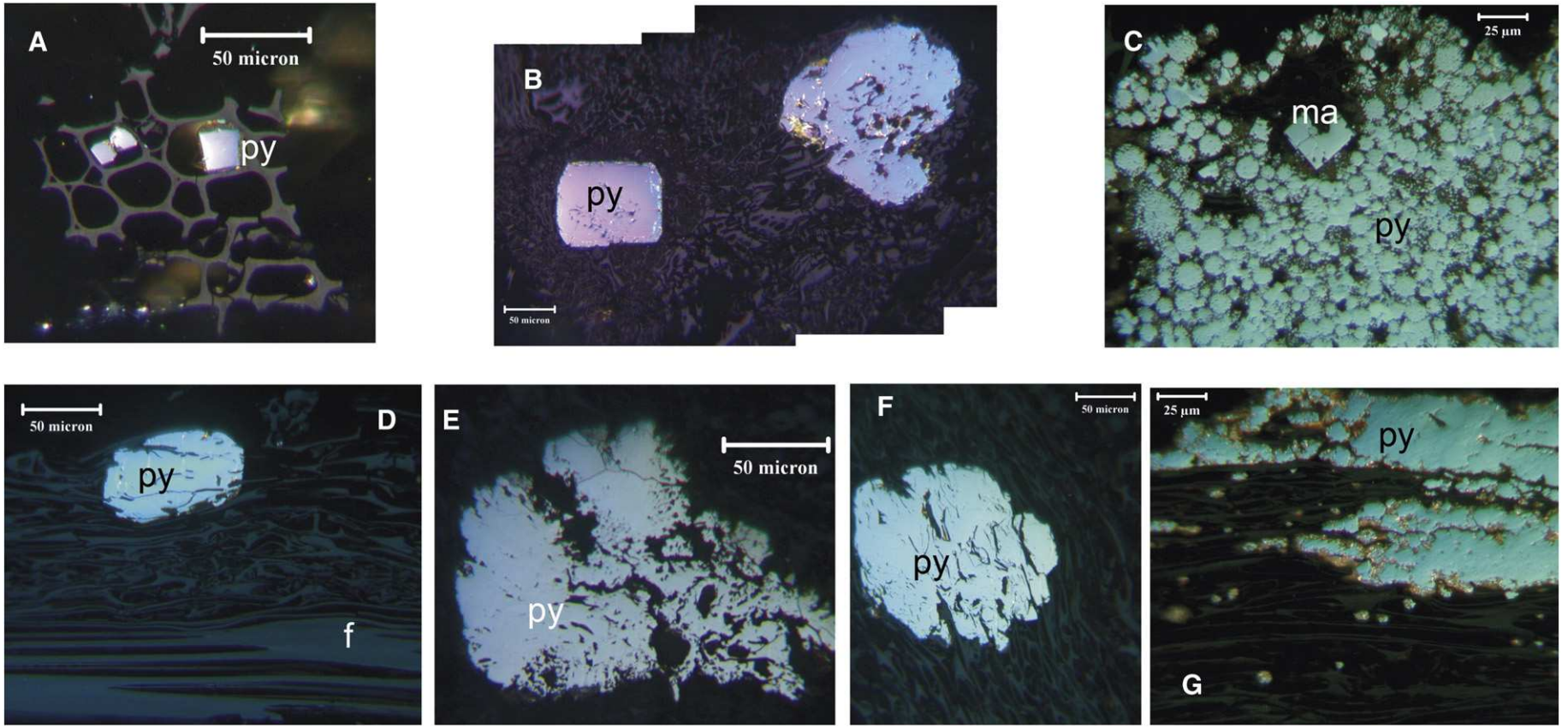

Fig. 15. Pyrite in the Wulantuga coal. Reflected light, oil immersion. (A) Euhedral pyrite (py) in fusinite lumens (photo 5 01; scale 50 microns). (B) Euhedral pyrite (py) in fusinite (photo 8 13; scale 50 microns). (C) Euhedral marcasite (ma) and framboidal pyrite (py) in fusinite (photo 11 04; scale 25 microns). (D) Euhedral pyrite (py) in fusinite lumen (f) (photo 9 01; scale 50 microns). (E) Massive pyrite (py) in fusinite (photo 4 07; scale 50 microns). (F) Massive pyrite (py) in fusinite. (photo 9 03; scale 50 microns). (G) Massive and framboidal pyrite (py) in fusinite (photo 10 07; scale 25 microns).

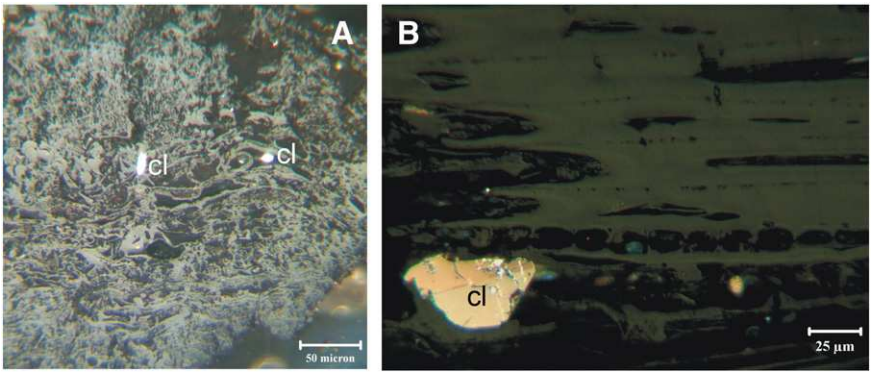

Fig. 16. Clausthalite in the Wulantuga coal. Reflected light, oil immersion. (A) Clausthalite (cl) in poorly indurated huminite macerals (photo 3 08; scale 50 microns). (B) Clausthalite in fusinite lumen (photo 11 01; scale 25 microns).

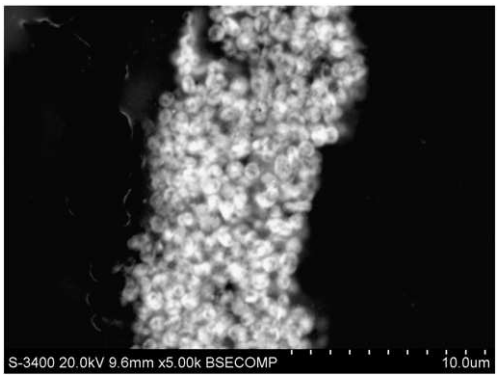

Fig. 17. Veined kaolinite in the Wulantuga Coal. SEM, electron backscattering images.

4.4.7. Rutile and anatase

Traces of rutile and anatase occur in the middle portion of the section studied, whereas they are, if present, below the XRD detection limit in the upper and lower portions. The rutile or anatase in sample C6-2 is distributed in and associated with the authigenic kaolinite (Fig. 20).

4.4.8. Ge-minerals

Although Zhuang et al. (2006) have found fine-grained Ge-minerals (oxides or oxalates) in the Wulantuga coals, Ge-bearing minerals were not detected in the present study by either microscope, SEM-EDX or XRD techniques in the bench samples and the corresponding LTAs.

4.5. Elemental composition

The concentrations of major and trace elements in the coal bench samples, in comparison to average values for Chinese coals and world low-rank coals, are listed in Table 6. Compared to these averages, the

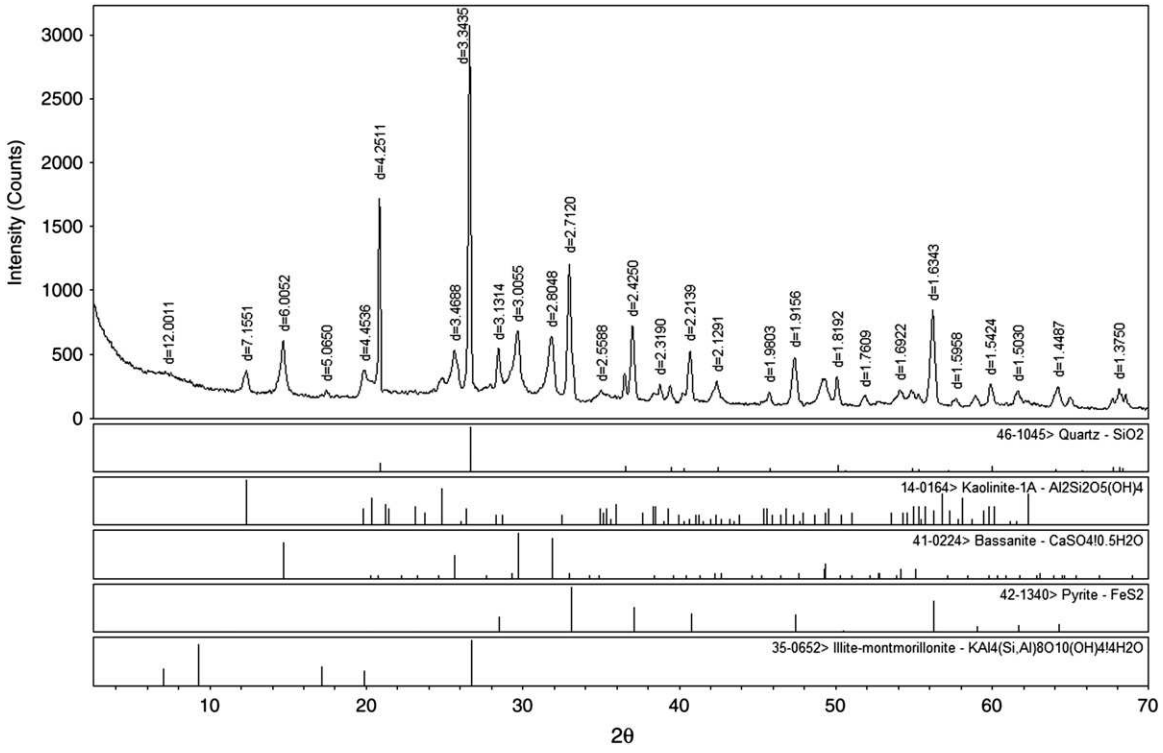

Fig. 18. Powder XRD pattern of the LTA of sample C6-11.

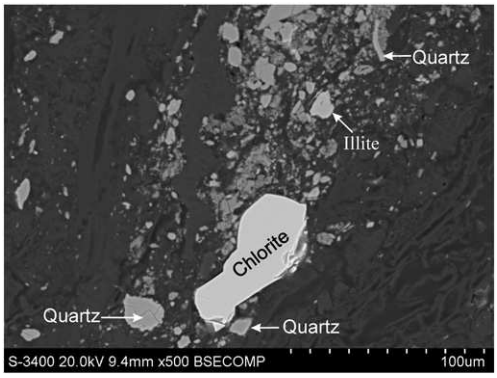

Fig. 19. Chlorite in the Wulantuga Coal. SEM, electron backscattering images.

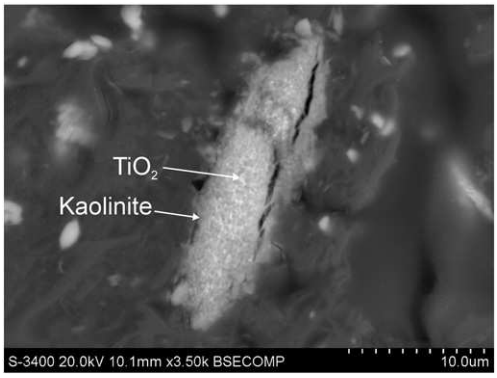

Fig. 20. Rutile or anatase distributes in the authigenic kaolinite. SEM, electron backscattering images.

coal from the Wulantuga Ge ore deposit displays a higher SiO_2/Al_2O_3 ratio (3.50) and higher values in Be (25.7 μg/g), F (336 μg/g), Ge (273 μg/g), As (499 μg/g), Sb (240 μg/g), Cs (5.29 μg/g), Hg (3.165 μg/g), Tl (3.15 μg/g), and W (115 μg/g). The concentrations of other trace elements are lower than those in most Chinese coals and world low-rank coals, and their concentration coefficients (CC, the concentration ratio of elements in the Wulantuga coals to the world low-rank coals) are less than 1 (Table 6; Fig. 21).

The assemblage of elements with elevated concentrations in the Wulantuga coals is similar to that in the Lincang Ge-rich coals in Yunnan, southwestern China, which contain 198 μg/g Be, 852 μg/g Ge, 47.6 μg/g As, 32.8 μg/g Sb, 22.7 μg/g Cs, and 375 μg/g W (on average; see Hu et al., 2009). A similar geochemical assemblage (Sb, W, Be, Cs, and As) is typical for the Spetzugli Ge-bearing coal deposit (Russian Far East) (Seredin, 2003a,b; Seredin and Finkelman, 2008).

4.5.1. Comparison between LTA Mineralogy and Sample Chemistry

Applying the methodology described by Ward et al. (1999), the chemical composition of the high-temperature coal ash expected to be derived from the mineral assemblage obtained from the Siroquant analysis was calculated for each LTA sample (Table 7). The methodology comprises calculations taking into account the loss of hydroxyl water from the clay minerals and CO_2 from the carbonates, as well as the conversion of pyrite to Fe_2O_3 and bassanite to anhydrite ($CaSO_4$) at the temperatures associated with high-temperature (815 °C) ashing and combustion processes.

Chemical data for the samples were recalculated to an LOI-free basis, with the sulfur converted to SO_3. The results were then normalized to indicate the concentrations of the major element oxides in the inorganic fraction of each coal sample (Table 8), rather than in each whole-coal sample. This would be expected to represent the chemical composition of the (high-temperature) ash derived from each coal sample.

The percentages of SiO_2, Al_2O_3, CaO, Fe_2O_3, K_2O, and SO_3 indicated by both sets of data (Tables 7 and 8) were plotted against each other (Fig. 22) to provide a basis for comparing the XRD results to the chemical analysis data for the same coal samples. As discussed for other materials by Ward et al. (1999, 2001), the respective data sets are presented as X-Y plots, with a diagonal line on each plot indicating where the points would fall if the estimates from the two different techniques were equal.

For SiO_2 and Al_2O_3, the points fall close to the equality line, suggesting that the percentages of quartz and the clay minerals indicated by the XRD analysis are consistent with the independently-determined chemical data. With the exception of the sample that appears to contain a significant amount of amorphous material (sample C6-3), the plots for CaO and SO_3 also fall close to the equality line, suggesting that the percentages of bassanite indicated by the XRD analysis are also consistent with the chemical data. The position of the data points for sample C6-3 on these plots suggest that the "amorphous" material in the LTA derived from that sample may include Ca and S which has not formed a crystalline bassanite phase.

Although broadly parallel, the points for Fe_2O_3 fall mostly below the equality line, suggesting that XRD analysis has under-estimated the proportion of Fe-bearing minerals in the coal samples. This apparent under-estimation may be due in part to the additional presence of amorphous Fe oxides within the LTA, which would not be detected by

Table 5
SEM-EDX semi-quantitative analysis for minerals and organic matter in the Wulantuga coal (wt. %).

Material		O	Na	Mg	Si	Al	K	Ca	S	Fe	As	W	Sb	Ti	Ge	Mn
Pyrite (N = 4)	Min	bdl	bdl	bdl	bdl	bdl	bdl	bdl	49.97	37.85	2.29	bdl	bdl	bdl	bdl	bdl
	Max	bdl	0.09	bdl	bdl	bdl	0.05	0.16	56.01	41.51	11.44	0.08	0.15	bdl	0.06	bdl
	Av	bdl	0.06	bdl	bdl	bdl	bdl	0.06	53.28	39.56	6.89	0.03	0.07	bdl	bdl	bdl
Cell-filling quartz (N = 3)	Min	54.05	0.09	0.06	37.76	bdl	0.04	0.04	bdl	0.24	0.04	bdl	bdl	bdl	bdl	bdl
	Max	59.78	0.32	0.11	43.73	bdl	0.04	0.23	bdl	0.55	0.16	1.36	bdl	bdl	bdl	bdl
	Av	56.46	0.19	0.08	41.45	bdl	bdl	0.11	bdl	0.4	0.09	0.82	bdl	bdl	bdl	bdl
Discrete quartz (N = 4)	Min	55.74	bdl	bdl	40.69	bdl	0.03	bdl	bdl	0.07	0.01	1	bdl	bdl	bdl	bdl
	Max	57.06	0.04	0.02	41.89	0.23	0.04	0.06	bdl	0.28	0.12	1.73	0.16	bdl	bdl	bdl
	Av	56.64	0.02	bdl	41.4	0.11	bdl	bdl	bdl	0.16	0.06	1.49	0.08	bdl	bdl	bdl
TiO_2 (N = 2)	Min	41.82	0.24	0.32	12.22	8.8	2.24	0.07	bdl	0.85	0.32	1.42	bdl	10.44	bdl	bdl
	Max	51.67	0.46	0.44	24.04	15.21	4.31	0.16	bdl	1.37	0.41	1.43	bdl	21.77	bdl	bdl
	Av	46.75	0.35	0.38	18.13	12.01	3.28	0.12	bdl	1.11	0.37	1.43	bdl	16.11	bdl	bdl
Chlorite (N = 2)	Min	47.18	0.05	6.21	17	10.39	bdl	0.57	bdl	14.96	0.02	1	0.01	bdl	bdl	bdl
	Max	48.93	0.21	6.32	17.76	10.8	bdl	0.69	bdl	15.72	0.09	1.15	0.03	bdl	bdl	0.28
	Av	48.06	0.13	6.27	17.38	10.6	bdl	0.63	bdl	15.34	0.06	1.08	0.02	bdl	bdl	0.14
Organic matter (N = 1)		bdl	0.09	0.11	bdl	0.13	0.02	0.33	0.54	0.07	0.04	0.11	0.03	bdl	0.09	bdl
Epigenetic Kaolinite (N = 1)		49.3	0.06	0.2	27.78	20.71	0.05	0.27	bdl	bdl	0.12	0.95	bdl	bdl	bdl	bdl

N, number of test spots; Min, minimum; Max, maximum; Av, average; bdl, below detection limit (0.01%).

Table 6
Elemental concentrations in coal bench samples from the Wulantuga Ore Deposit (elements in μg/g, oxides in %; on whole-coal basis).

	C6-1	C6-2	C6-3	C6-4	C6-5	C6-6	C6-7	C6-8	C6-9	C6-10	C6-11	C6-12	C6-13	WA	China [a]	World [b]	CC [c]
LOI	81.45	90.23	95.84	92.61	91.93	91.92	83.96	90.32	87.56	91.92	93.09	89.71	90.95	90.32	nd	nd	nd
Na_2O	0.13	0.12	0.09	0.12	0.07	0.06	0.06	0.08	0.05	0.05	0.13	0.05	0.17	0.09	0.16	nd	nd
MgO	0.44	0.25	0.22	0.29	0.24	0.24	0.35	0.20	0.27	0.23	0.23	0.18	0.37	0.27	0.22	nd	nd
Al_2O_3	3.51	1.05	0.49	0.82	1.28	1.27	2.54	1.35	2.86	0.76	0.60	1.26	0.59	1.38	5.98	nd	nd
SiO_2	10.05	4.23	0.75	2.10	3.61	3.59	9.34	4.11	5.12	2.79	2.00	5.76	4.13	4.18	8.47	nd	nd
SiO_2 /Al_2O_3	2.86	4.02	1.52	2.56	2.83	2.83	3.68	3.04	1.79	3.69	3.32	4.58	7.04	3.50	1.42	nd	nd
K_2O	0.267	0.079	0.021	0.027	0.036	0.036	0.141	0.022	0.035	0.016	0.030	0.058	0.047	0.052	0.19	nd	nd
CaO	0.69	0.57	0.64	0.74	0.80	0.81	1.04	0.62	0.84	0.83	0.66	0.52	0.54	0.70	1.23	nd	nd
TiO_2	0.135	0.067	0.021	0.034	0.049	0.048	0.167	0.077	0.076	0.072	0.035	0.090	0.030	0.063	0.33	0.12	0.53
Fe_2O_3	2.18	2.18	0.76	2.06	0.82	0.82	1.03	2.19	2.00	1.99	2.01	1.48	1.80	1.77	4.85	nd	nd
Li	13.3	5.27	1.94	4.16	5.75	5.78	11.5	8.14	15.2	4.88	3.38	6.59	6.49	7.35	31.8	10	0.74
Be	19.0	18.6	14.9	26.4	29.6	29.9	45.6	22.4	33.8	31.8	20.2	20.6	24.5	25.7	2.11	1.2	21.4
F	1004	231	175	158	166	463	375	300	534	226	215	273	239	336	130	90	3.73
P	35.6	5.16	2.45	4.55	17.1	12.1	30.0	47.34	163	5.33	5.64	15.2	4.31	33.7	402	200	0.17
Sc	4.31	1.96	1.35	0.90	1.34	1.25	2.52	1.17	1.66	0.90	0.56	0.92	1.16	1.39	4.38	4.1	0.34
V	24.1	7.53	4.26	4.97	7.61	7.18	19.5	8.17	8.99	7.77	5.20	10.2	5.56	8.42	35.1	22	0.38
Cr	16.5	6.02	2.86	3.44	4.95	4.42	17.0	5.86	7.33	5.42	4.13	6.71	6.07	6.31	15.4	15	0.42
Mn	39.8	36.4	26.5	42.0	46.0	47.3	56.7	40.9	53.1	55.4	43.3	36.8	61.6	46.5	116	100	0.47
Co	3.72	1.47	1.14	1.18	0.70	1.16	0.78	1.96	1.19	2.87	3.02	3.13	7.91	2.66	7.08	4.2	0.63
Ni	7.85	4.05	3.45	3.75	1.95	3.62	2.34	5.29	3.25	5.95	4.30	5.26	7.20	4.73	13.7	9	0.53
Cu	19.7	4.53	3.84	4.09	3.33	3.19	15.28	6.22	5.60	4.46	3.49	4.99	3.67	5.57	17.5	15	0.37
Zn	11.6	4.80	4.08	4.69	4.56	4.34	8.77	9.44	13.3	9.35	10.5	17.5	47.0	13.7	41.4	18	0.76
Ga	5.60	1.68	1.13	1.10	1.21	1.15	3.96	3.22	3.68	1.79	9.50	8.58	10.8	4.59	6.55	5.5	0.83
Ge	290	797	1170	340	168	143	64.0	187	45.0	51.3	372	269	376	273	2.78	2	137
As	497	878	623	542	209	208	145	549	466	494	666	624	473	499	3.79	7.6	65.6
Se	0.40	0.17	0.05	0.08	bdl	0.15	0.29	0.24	0.41	bdl	1.28	1.36	1.12	0.49	2.47	1	0.49
Rb	28.34	6.98	2.16	1.97	7.31	3.80	12.75	2.61	3.29	1.55	2.27	4.22	3.40	5.08	9.25	10	0.51
Sr	53.5	45.0	45.6	49.5	50.2	50.9	67.4	49.7	109	42.5	38.6	32.4	38.6	53.1	140	120	0.44
Zr	33.6	11.3	3.30	6.46	10.5	10.1	30.2	31.1	58.1	16.7	9.60	18.5	8.62	20.8	89.5	35	0.59
Nb	2.26	0.71	0.17	0.37	0.73	0.67	2.67	1.83	3.52	1.23	0.90	1.30	0.54	1.35	9.44	3.3	0.41
Mo	1.36	0.59	0.80	0.67	0.28	0.26	0.17	0.63	0.51	0.26	1.12	1.43	1.78	0.82	3.08	2.2	0.37
Ag	0.16	0.08	0.03	0.03	0.04	0.08	0.12	0.11	0.16	0.05	0.06	0.08	0.04	0.08	nd	0.09	0.90
Cd	0.152	0.028	0.016	0.028	0.042	0.036	0.096	0.054	0.104	0.052	0.028	0.040	0.026	0.053	0.25	0.24	0.22
In	0.024	0.006	0.004	0.004	0.008	0.004	0.026	0.006	0.012	0.008	0.004	0.006	0.002	0.007	0.047	0.021	0.35
Sn	0.82	0.16	0.17	0.16	0.21	0.29	0.81	0.27	0.46	0.24	0.04	0.37	0.09	0.28	2.11	0.79	0.35
Sb	14.7	42.1	53.7	18.8	6.7	6.0	9.7	197	106	92.4	645	617	693	240	0.84	0.84	285
Cs	23.5	7.26	4.87	3.89	3.65	3.55	9.03	3.67	3.82	2.67	4.19	4.65	3.94	5.29	1.13	0.98	5.40
Ba	193	225	23.0	20.1	15.1	14.7	38.4	30.9	114	12.6	172	20.7	17.0	66.0	159	150	0.44
Hf	0.92	0.32	0.08	0.18	0.29	0.28	0.92	0.75	1.42	0.42	0.24	0.48	0.22	0.53	3.71	1.2	0.44
Ta	0.12	0.04	0.01	0.01	0.02	0.02	0.34	0.09	0.15	0.08	0.05	0.08	0.03	0.07	0.62	0.26	0.27
W	205	362	514	201	85.0	92.8	52.6	73.6	21.1	40.3	83.5	81.3	86.8	115	1.08	1.2	95.8
Hg	1.693	2.118	0.767	1.890	0.648	0.653	0.744	4.630	3.807	4.456	6.644	2.766	3.950	3.165	0.163	0.1	31.7
Tl	1.39	0.97	0.26	0.68	0.40	0.65	0.38	5.69	4.01	4.50	5.91	3.46	4.50	3.15	0.47	0.68	4.63
Pb	8.47	1.65	0.99	1.59	2.02	1.88	5.09	1.89	6.32	1.91	1.42	1.86	1.07	2.69	15.1	6.6	0.41
Bi	0.26	0.03	0.03	0.01	0.05	0.02	0.14	0.04	0.05	0.02	0.01	0.03	0.01	0.04	0.79	0.84	0.05
Th	3.89	0.94	0.52	0.52	1.18	0.90	4.35	1.35	2.19	1.40	0.82	1.29	0.59	1.35	5.84	3.3	0.41
U	1.02	0.35	0.31	0.24	0.27	0.27	0.72	0.31	0.39	0.31	0.22	0.39	0.32	0.36	2.43	2.9	0.12

LOI, loss of ignition; WA, weighted average; nd, no data; bdl, below detection limit; [a], Average concentrations of elements in the common Chinese coals (Dai et al., 2011a); [b], Average concentrations of elements in the world low-rank coals (Ketris and Yudovich, 2009); [c],CC, ratio of concentrations of elements in the Wulantuga coals to the world low-rank coals.

the XRD analysis. Such material may, for example, represent Fe in the pore water or in the organic matter, which did not form crystalline phases during air-drying or low-temperature ashing.

Many of the data points on the plot for K_2O are also close to the equality line. The data for two samples, however, lie well above the line, suggesting that, although the samples in question (C6-1 and C6-9) contain a high proportion of illite (Table 3), the illite does not contain as much K as might be expected for an illite fully-saturated with K in its interlayer spaces (cf. Ward et al., 1999). A few other points plot on the X-axis; these are samples for which illite was not detected by the XRD analysis but in which small concentrations of illite may be indicated by the chemical analysis.

The pyrite content of each whole-coal sample (i.e. including the organic matter) was calculated from the XRD data for the LTA samples in conjunction with the respective LTA yields. The results were plotted against the pyrite contents in the same sample, as indicated by the (separately-determined) pyritic sulfur values. The results (Fig. 23) indicate that data for many of the samples plots close to the diagonal equality line, suggesting consistency in the two different determinations. Among the samples plotting as outliers are samples C6-6 and C6-10, which showed inconsistency when the percentages of pyrite from whole-coal and LTA were compared and may have been affected by segregation in preparation. The other prominent outlier is sample C6-03, for which the LTA had a high proportion of amorphous material.

4.5.2. Major elements

The major element oxides in coals from the Wulantuga Mine are dominated by Al_2O_3, SiO_2, and Fe_2O_3 (Table 6), which occur at lower concentrations than those in most Chinese coals reported by Dai et al. (2011a). With the exception of MgO with a weighted average 0.27%, which is close to that in most Chinese coals (0.22%), the concentrations of Na_2O, CaO, P_2O_5, and TiO_2 in the No.6 Coal are lower in comparison with those in other Chinese coals.

In addition to a proportion of Si in clay minerals (kaolinite, illite/smectite, and chlorite), silicon also occurs in quartz. Clay minerals are the major carriers of Al in the coal samples.

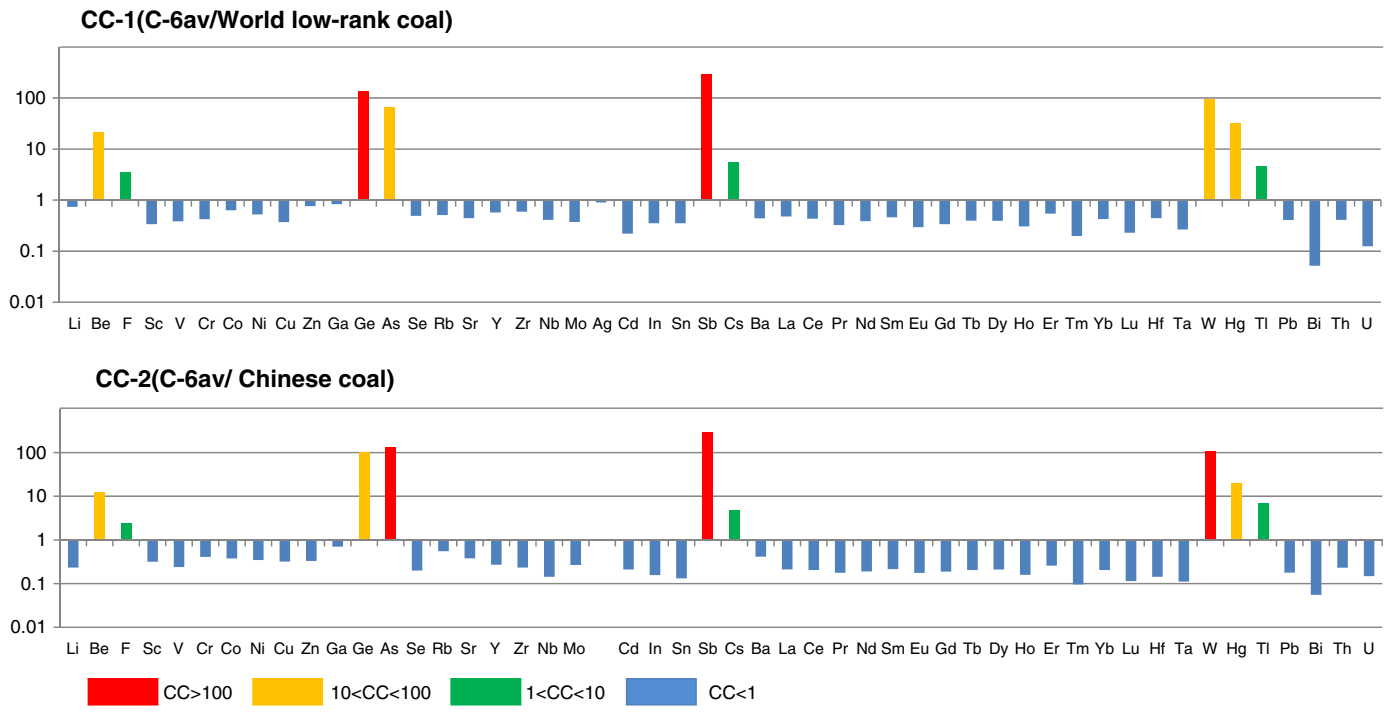

Fig. 21. Concentration coefficients of trace elements in the Wulantuga coals vs. the world low-rank (A) and Chinese coals (B).

The SiO_2/Al_2O_3 ratio for each bench sample of the No.6 Coal (3.50 on average) is higher than the same ratio for kaolinite (1.18) and also than common values in Chinese coals (1.42; see Dai et al., 2011a). The variation of SiO_2/Al_2O_3 in the No.6 Coal is consistent with the variation in mineralogical composition.

The correlation coefficients of Fe-S_t and Fe-S_p are 0.91 and 0.95, respectively (Table 9), indicating that Fe mainly occurs in pyrite.

Calcium is associated with both the gypsum and the organic matter. As discussed above, the organically-associated Ca partially interacted with S during oxidation of the organic matter to form

Table 7
Inferred chemical composition of coal ash (wt. %) calculated from XRD analysis of LTA residues.

Sample	SiO_2	TiO_2	Al_2O_3	Fe_2O_3	MgO	CaO	Na_2O	K_2O	P_2O_5	SO_3	Total
C6-1	60.18	0.00	29.21	3.99	0.00	1.05	0.00	4.06	0.00	1.50	100.00
C6-2	55.52	0.00	14.37	13.75	0.00	6.27	0.00	1.11	0.00	8.97	100.00
C6-3	43.85	0.00	14.19	21.18	0.00	8.30	0.00	0.61	0.00	11.87	100.00
C6-4	38.54	0.00	12.81	20.02	0.00	11.54	0.00	0.60	0.00	16.50	100.00
C6-5	51.27	0.33	16.24	5.95	0.00	10.62	0.00	0.40	0.00	15.19	100.00
C6-6	39.11	0.69	10.36	18.88	0.00	12.74	0.00	0.00	0.00	18.22	100.00
C6-7	62.28	0.65	17.65	3.47	0.00	6.18	0.00	0.92	0.00	8.84	100.00
C6-8	49.06	0.00	14.56	16.78	0.00	8.07	0.00	0.00	0.00	11.54	100.00
C6-9	50.17	1.14	31.21	7.51	0.00	3.34	0.00	1.86	0.00	4.77	100.00
C6-10	51.09	0.22	16.56	5.73	0.00	10.71	0.00	0.38	0.00	15.32	100.00
C6-11	40.58	0.00	9.78	20.33	0.13	11.76	0.10	0.62	0.00	16.70	100.00
C6-12	65.01	0.00	14.19	7.18	0.00	5.29	0.00	0.76	0.00	7.57	100.00
C6-13	59.17	0.00	4.92	16.40	0.00	8.03	0.00	0.00	0.00	11.48	100.00

Table 8
Normalised chemical composition of coal ash (wt. %; LOI-free) based on chemical analysis data, with S expressed as SO_3.

Sample	LTA yield	SiO_2	Al_2O_3	Fe_2O_3	CaO	MgO	MnO	Na_2O	K_2O	P_2O_5	TiO_2	SO_3	Total
C6-1	29.53	54.69	19.11	11.87	3.77	2.37	0.03	0.68	1.45	0.04	0.74	5.25	100.00
C6-2	13.91	44.64	11.11	22.99	6.03	2.62	0.05	1.29	0.84	0.01	0.71	9.70	100.00
C6-3	8.71	19.43	12.78	19.72	16.65	5.71	0.09	2.24	0.55	0.01	0.53	22.29	100.00
C6-4	11.38	29.11	11.36	28.54	10.22	3.97	0.08	1.68	0.38	0.01	0.46	14.21	100.00
C6-5	10.39	45.17	15.98	10.32	10.04	2.98	0.07	0.93	0.46	0.05	0.61	13.39	100.00
C6-6	11.09	44.84	15.83	10.23	10.17	2.97	0.08	0.79	0.45	0.03	0.60	14.01	100.00
C6-7	21.11	58.50	15.89	6.43	6.49	2.19	0.05	0.38	0.88	0.04	1.04	8.11	100.00
C6-8	12.61	43.12	14.17	23.03	6.46	2.09	0.06	0.85	0.23	0.11	0.80	9.07	100.00
C6-9	19.87	41.58	23.21	16.21	6.78	2.20	0.06	0.40	0.29	0.30	0.62	8.35	100.00
C6-10	10.15	35.05	9.50	24.91	10.42	2.92	0.09	0.60	0.20	0.02	0.91	15.40	100.00
C6-11	8.47	29.88	9.00	30.12	9.80	3.51	0.08	1.98	0.44	0.02	0.52	14.63	100.00
C6-12	11.92	57.02	12.45	14.62	5.12	1.74	0.05	0.50	0.58	0.03	0.89	7.01	100.00
C6-13	10.64	46.66	6.63	20.35	6.08	4.23	0.09	1.89	0.53	0.01	0.34	13.19	100.00

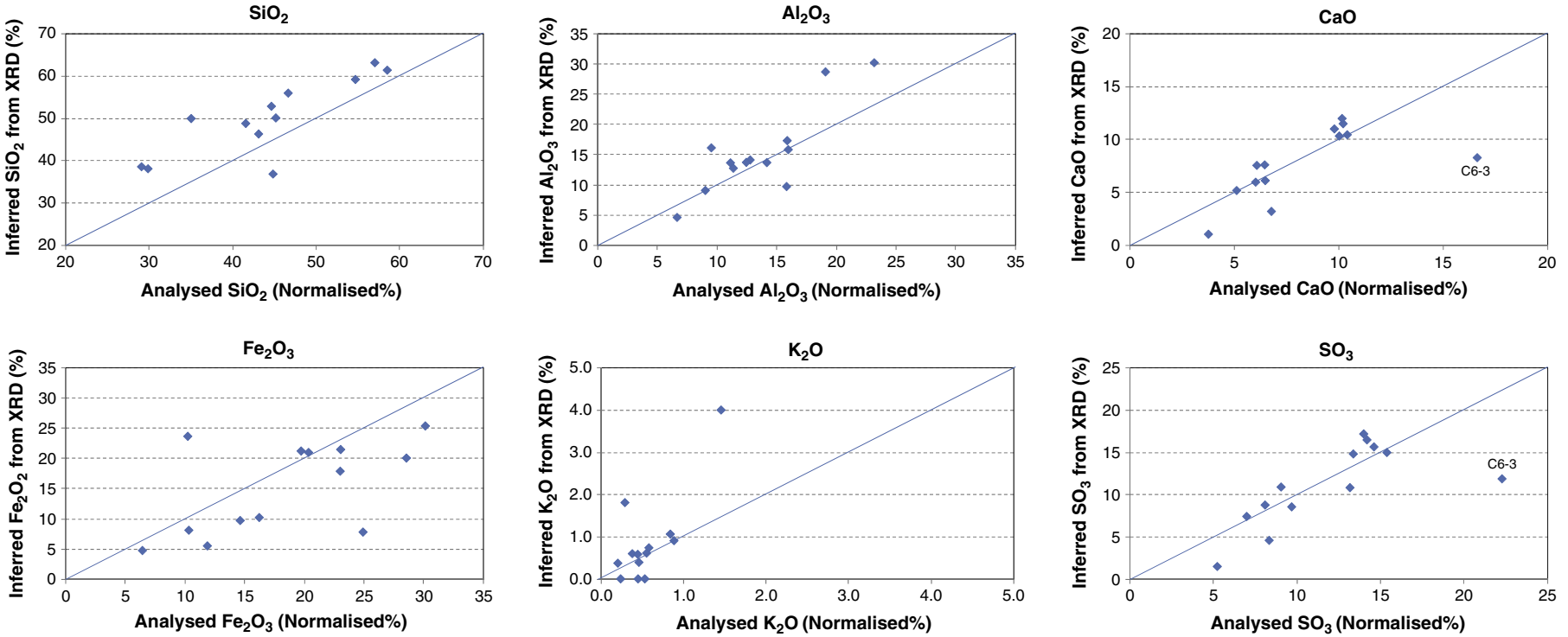

Fig. 22. Comparison of observed normalised oxide percentages from chemical analysis (x-axis) to oxide percentages for sample ash inferred from XRD data (y-axis). The diagonal line in each plot indicates equality.

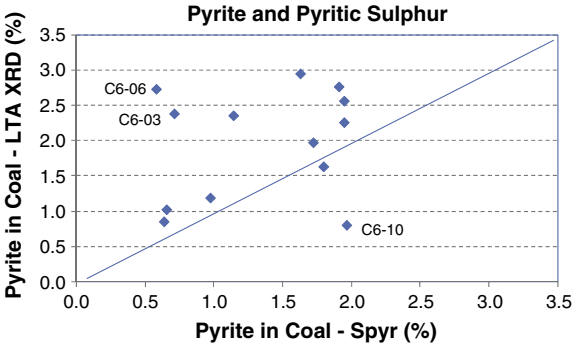

Fig. 23. Comparison of pyrite as a fraction of each coal sample, determined from pyritic sulfur (Spyr) vs calculated from XRD analysis of LTA residues combined with LTA percentage.

bassanite. Titanium is contained in rutile in most bench samples and a proportion is in anatase in sample C6-9.

4.5.3. Elevated trace elements in the coal

4.5.3.1. Germanium. The average concentrations of Ge in common Chinese coals and world low-rank coals are 2.78 μg/g and 2.0 μg/g, respectively (Dai et al., 2011a; Ketris and Yudovich, 2009). Germanium is significantly enriched in the Wulantuga coals, from 45.0 to 1170 μg/g along the section in this study, with a weighted average of 273.4 μg/g, being 98.2 and 137 times the Chinese and world low-rank coal averages, respectively.

Based on 12 bench samples, Zhuang et al. (2006) showed that Ge varies from 22 to 1894 μg/g (average 427 μg/g) and is significantly concentrated in the central portion of the section. The Ge concentration varies from 23.3 to 1424 μg/g, with geometric and arithmetic mean values of 168 and 300 μg/g (Qi et al., 2007a). Du et al. (2009) showed that the Ge concentration in the coal ranges from 32 to 820 μg/g, with a mean value of 137 μg/g (on a bulk coal basis, mean of 939 coal samples from 75 boreholes in the No.6 coal seam) over an area of 2.2 km^2.

The above data indicate that the lateral distribution of Ge concentration greatly varies in the Wulantuga ore deposit. However, it follows a fan-shaped trend, decreasing from the SW to the NE of the coal field, with a sharp gradient of Ge concentration at the southern margin of the deposit (Du et al., 2009). Moreover, the vertical distribution of Ge concentration markedly varies, being concentrated in the lower and upper portions of the section studied, and has an inverse variation with ash yield (Fig. 24). However, Ge enrichment may also occur in the middle portion (Zhuang et al., 2006); Du et al. (2004, 2009) indicating that the element can be enriched in the lower, middle, and upper portions of the coal seam. Based on the vertical variation of Ge, Du et al. (2004) suggested that the Ge concentration in the Wulantuga Ge-rich coal does not obey "Zilbermints Law" (Pavlov, 1966; Yudovich, 2003; Zilbermints et al., 1936), which suggested that Ge enrichment occurs near the bottom, roof, and partings of the coal seam.

The correlation coefficient of Ge-ash is very low (−0.44), suggesting that Ge is mainly associated with the organic matter. The mode of Ge occurrence in the Wulantuga ore deposit from the present study is consistent with that reported by Zhuang et al. (2006) and Qi et al. (2007a), although some minor fine-grained Ge-bearing minerals have been observed (Zhuang et al., 2006). Germanium in the Ge-rich coals from Lincang (Yunnan, China) and Spetzugli (Far East, Russia) is associated with organic matter, and no fine-grained Ge-bearing minerals have been found in these Ge ore deposits (Hu et al., 2009; Qi et al., 2004; Seredin, 2003a,b).

As pointed out by some authors (Du et al., 2009; Qi et al., 2004; and Zhuang et al., 2006), the enrichment of Ge in the Wulantuga coals has been attributed to hydrothermal fluids circulating through the fault systems, probably from the adjacent granitoids. The

Table 9
Element affinities deduced from calculation of Pearson's correlation coefficients between the content of each element in coal and ash yield or selected elements.

Correlation with ash yield
- Group 1: r_{ash} = 0.7- 1.0 MgO (0.70), Al_2O_3 (0.93), SiO_2 (0.97), K_2O (0.87), TiO_2 (0.89), Li (0.88), F (0.81), Sc (0.86), V (0.94), Cr (0.95), Cu (0.91), Rb (0.84), Y (0.72), Nb (0.77), Ag (0.86), Cd (0.92), In (0.90), Sn (0.91), Cs (0.78), REE (La-Lu, 0.79-0.90), Hf (0.77), Ta (0.75), Pb (0.90), Bi (0.87), Th (0.92), U (0.91)
- Group 2: r_{ash} = 0.40 - 0.69 P_2O_5 (0.42), Sr (0.44), Zr (0.69)
- Group 3: r_{ash} = 0.20 -0.39 CaO (0.34), MnO (0.28), Be (0.37), Ni (0.25), Ba (0.38)
- Group 4: r_{ash} = − 0.20 - 0.19 Na_2O (−0.05), Co (0.06), Zn (0.09), Ga (0.16), Mo (0.06), Se (−0.07), Hg (−0.18), Tl (−0.13)
- Group 5: r_{ash} < −0.2 Ge (−0.44), As (−0.28), Sb (−0.23), W (−0.29)

Aluminosilicate affinity
- r_{Al-Si} > 0.7 K_2O, Li, F, Sc, V, Cr, Cu, Rb, Ag, Cd, In, Sn, Cs, REE, Pb, Bi, Th, U
- r_{Al-Si} < −0.35 Ge

Carbonate affinity
- r_{Ca} > 0.7 Be (0.87)
- r_{Ca} > 0.5-0.69 Sr (0.57), In (0.58), Sn (0.51), Th (0.56), Hf (0.63)
- r_{Ca} > 0.35-0.49 Al_2O_3 (0.43), TiO_2 (0.46), MnO (0.47), Li (0.38), V (0.36), Cr (0.41), Zr (0.35), Nb (0.46), Cd (0.42), La (0.45), Ce (0.42), Pr (0.38), Pb (0.42)
- r_{Ca} < −0.35 Fe_2O_3 (−0.35), Na_2O (−0.51), Co (−0.53), Ni (−0.53), Zn (−0.40), Ga (−0.45), Ge (−0.52), As (−0.75), Se (−0.45), Mo (−0.76), Sb (−0.60), W (−0.36).

Sulfate/sulfur affinity
- r_s > 0.7 Fe_2O_3 (0.91), As (0.74)
- $r_{pyrite\ sulfur}$ = 0.5–0.69 Ni (0.56), Ba (0.57), Hg (0.56)
- $r_{pyrite\ sulfur}$ = 0.35–0.49 Co (0.43), Y (0.39), Mo (0.49)
- $r_{pyrite\ sulfur}$ < 0.35 other elements

Phosphate affinity
- r_P > 0.7 Li (0.78), Sr (0.92), Zr (0.91), Nb (0.83), Ag (0.73), La (0.82), Ce (0.77), Pr (0.72), Tm (0.70), Hf (0.87)
- r_P = 0.5-0.69 Al_2O_3 (0.64), Y (0.51), Cd (0.57), Nd (0.69), Sm (0.68), Gd (0.65), Tb (0.68), Dy (0.69), Ho (0.67), Er (0.67), Yb (0.69), Lu (0.65), Pb (0.61)
- r_P = 0.35-0.49 Be (0.33), F (0.42), Sn (0.38), Tb (0.36)
- r_P < −0.35 Ge (−0.39), W (−0.35)

Correlation coefficients between selected elements
- SiO_2–Al_2O_3 = 0.86;
- F – Al_2O_3 = 0.86, F – SiO_2 = 0.75, F – K_2O = 0.82, F-Ge = −0.27
- Cs-K_2O = 0.97, Cs –SiO_2 = 0.72, Cs-Al_2O_3 = 0.75
- Hg-Ge = −0.2, Hg-Fe = 0.58, Hg-Tl = 0.95, Hg-Sb = 0.65
- Ge-W = 0.95, Ge-Hg = −0.20 Ge-Tl = −0.31, Ge- As = 0.61 Ge-Sb = 0.00, Ge-Fe = −0.27
- W-Hg = −0.40, W-Tl = −0.51, W-As = 0.51, W-Sb = −0.28
- As-Hg = 0.45, As-Tl = 0.32, As-Sb = 0.32
- Tl-Sb = 0.69

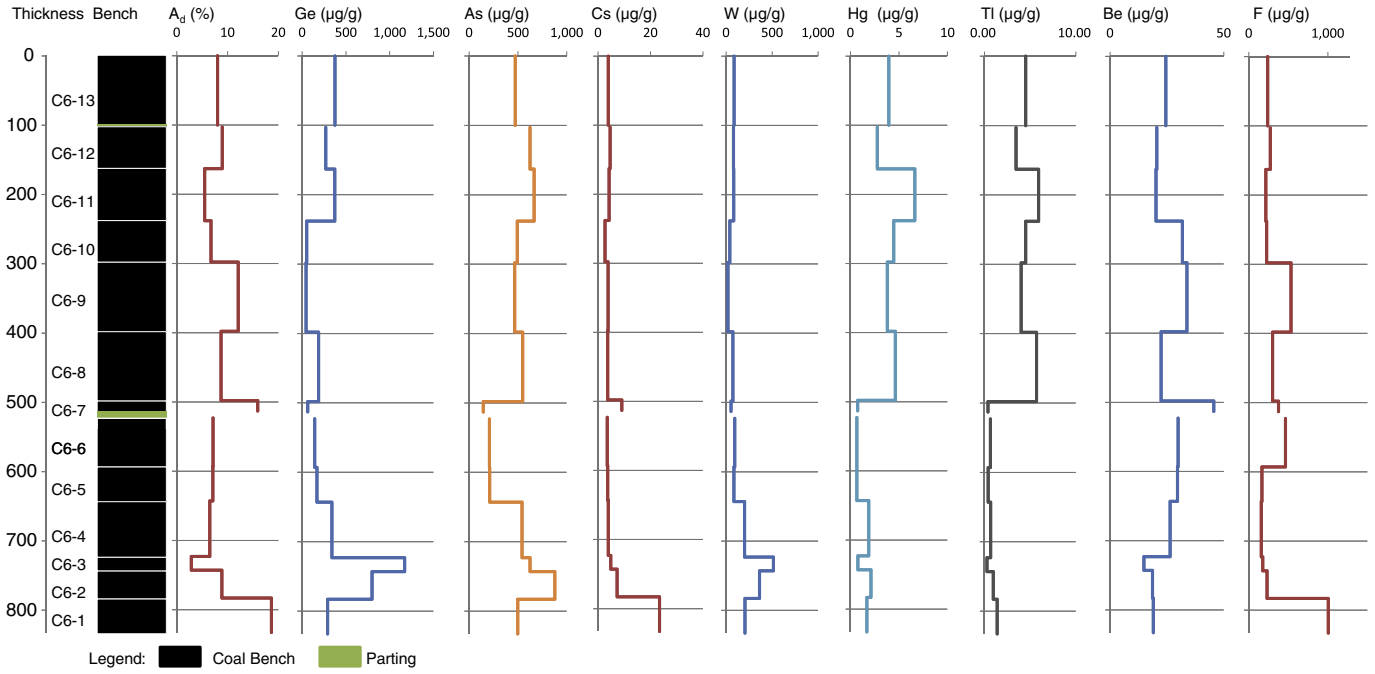

Fig. 24. Content variations of trace elements (Ge, Be, As, Cs, W, Hg, Tl, and F) along the coal seam profile.

Ge-rich hydrothermal fluids circulated through the buried organic matter, which adsorbed Ge during the diagenetic stage.

4.5.3.2. Beryllium. The Be concentration varies from 14.9 to 45.6 μg/g along the section in this study, with a weighted average of 25.7 μg/g, much higher than averages in other Chinese and world low-rank coals (2.11 and 1.2 μg/g, respectively), as reported by Dai et al. (2011a) and Ketris and Yudovich (2009). Beryllium has an inverse variation with Ge along the section and is concentrated in the middle portion of the seam (Table 6, Fig. 24).

Owing to its low abundance in coal and its low atomic number, there is no direct evidence of the mode of occurrence of Be in coals, and in many coal deposits this has been deduced by indirect evidence, such as statistics and density fractions (Eskenazy, 2006; Eskenazy and Valceva, 2003; Kolker and Finkelman, 1998; Kortenski and Sotirov, 2002). It has been proposed that Be in coal probably has both organic and clay mineral associations (Eskenazy, 2006; Kolker and Finkelman, 1998). Moreover, if the Be content in coal is high, it is predominantly organically bound, whereas the inorganic form prevails in coal when the Be concentration approximates the Clarke values (Eskenazy, 2006).

However, the correlation coefficients of Be-ash (0.37), Be-Ge (−0.70), Be-As (−0.76), Be-Mo (−0.60), and Be-W (−0.63) indicate that the Be in the present study mainly has an inorganic affinity, although Be is significantly elevated in the coal. A large proportion of the Ge, As, Mo, and W is associated with organic matter (modes of occurrence of As, Mo and W are described below). In addition, the high correlation coefficients for Be-CaO (0.87) and Be-MnO (0.74), but low coefficients for Be-Al_2O_3 (0.36) and Be-SiO_2 (0.36), suggest that Be is mainly associated with Ca- and Mn-bearing carbonate minerals and to a lesser extent with clay minerals.

4.5.3.3. Fluorine. The average concentration of fluorine in most Chinese and world low-rank coals is 130 and 90 μg/g, respectively (Dai et al., 2011a; Ketris and Yudovich, 2009). However, it is much higher in the Wulantuga coals, varying from 158 to 1004 μg/g with a weighted average of 336 μg/g. Fluorine is concentrated in the middle portion and the lowermost C6-1 bench (Fig. 24), in accordance with ash yield variation but with an inverse relationship with Ge (Fig. 24).

Fluorine commonly occurs in minerals such as clays and fluorapatite, and less commonly in fluorite, tourmaline, topaz, amphiboles, micas, gorceixite, and boehmite (Dai et al., 2011c; Finkelman, 1995; Godbeer and Swaine, 1987; Swaine, 1990). In addition, fluorine may have an organic affinity (Bouška et al., 2000; Dai et al., 2011a; McIntyre, 1985; Wang et al., 2011).

The correlation coefficient between F and ash yield is 0.81, indicating that fluorine has an inorganic affinity in the present study. The positive correlation coefficients of F – Al_2O_3 (0.86), F – SiO_2 (0.75), and F – K_2O (0.82) indicate that F largely occurs in the clay minerals (kaolinite and illite).

4.5.3.4. Thallium. Generally, Tl is at a low level in coals, for example, with averages of 0.47 and 0.68 μg/g in most Chinese coals (Dai et al., 2011a) and world low-rank coals (Ketris and Yudovich, 2009), respectively. The concentration of Tl in the Wulantuga coals is much higher, varying from 0.26 to 5.91 μg/g and averaging 3.15 μg/g. The concentration of Tl is low in bench samples C6-1 to C6-7, but sharply increases in the middle and upper portions of the section (C6-8 to C6-13; Fig. 24).

The mode of occurrence of Tl in coal has not been studied in great detail. It is generally considered that Tl in coal is mainly present in sulfides (Dai et al., 2006; Finkelman, 1995; Hower et al., 2005b, 2008). Zhuang et al. (2007) found a statistical relationship between Tl and Al–Si minerals in Late Permian coals from Hubei, China. The high correlation coefficients of Tl-S_p (0.58) and Tl-Fe_2O_3 (0.58) in the Wulantuga coals indicate that Tl mainly occurs in pyrite.

4.5.3.5. Mercury. Despite its low level of abundance in coal, the concentration and mode of occurrence of mercury in coal are of growing concern due to its toxic effects and its tendency to bioaccumulate through the food chain (Yudovich and Ketris, 2005b). It is generally considered that Hg in coal is primarily present in pyrite, or other sulfides (Hower et al., 2008), although some studies indicated that Hg also occurs in calcite and chlorite (Zhang et al., 2002), clausthalite (Hower and Robertson, 2003), kleinite and cinnabar (Brownfield et al., 2005), and getchellite (Dai et al., 2006).

The concentration of Hg in the Wulantuga coals is very high, averaging 3.165 μg/g. Its average concentration is 19.4 and 31.7

times respectively higher than in the Chinese and world low-rank coals reported by Dai et al. (2011a) and Ketris and Yudovich (2009), and close to the data (mean 4 μg/g) for the Wulantuga coal reported by Zhuang et al. (2006).

The vertical variation of Hg is similar to that of Tl (Fig. 24), being enriched in the middle and upper portions of the seam as described above. The high correlation coefficients of Hg-$S_{p,d}$ (0.70) and Hg-Fe (0.58) indicate that Hg, like Tl, mainly occurs in pyrite. The similarity in the vertical variations and the modes of occurrence of Tl and Hg is thought to indicate the same source.

4.5.3.6. Arsenic. Both the modes of occurrence and the abundance of As in coal have been investigated in detail, due to its high toxicity and adverse impact on human health. The average As concentration of common Chinese and world low-rank coals are 3.79 (Dai et al., 2011a) and 7.6 μg/g (Ketris and Yudovich, 2009), respectively. The weighted average concentration of As in the Wulantuga bench samples is as high as 499 μg/g, 131.2 and 65.6 times higher than that in Chinese and world low-rank coals, and up to 3791 times higher (on an ash basis) than that of the upper crustal Clarke value reported by Taylor and McLennan (1985).

Previous studies have shown that As in coal is generally associated with pyrite, commonly as As-rich inclusions in the pyrite lattice (Coleman and Bragg, 1990; Eskenazy, 1995; Hower et al., 1997; Huggins and Huffman, 1996; Minkin et al., 1984; Ruppert et al., 1992; Ward, 2001; Ward et al., 1999; Yudovich and Ketris, 2005a). Arsenic is also associated with Ti-As sulfide (Hower et al., 2005a,b); getchellite (Dai et al., 2006); clay minerals (Swaine, 1990); phosphate minerals (Swaine, 1990); and arsenic minerals including orpiment, realgar, and arsenopyrite (Ding et al., 2001). The low As–A_d (−0.28) and high Ge-As (0.61) correlation coefficients indicate that a proportion of the As is associated with the organic matter. Occurrences of organically associated As have also been reported in some other coals (Belkin et al., 1997; Zhao et al., 1998). However, the high correlation coefficients of As-$S_{p,d}$ (0.64) and As-Fe_2O_3 (0.60) in the present study show that As also occurs in pyrite. SEM-EDX data showed that pyrite contains 8.8% As (ranging from 2.29 to 11.44%) (Table 5).

4.5.3.7. Tungsten. Tungsten usually is at a low level in coal (Chinese coals, 1.08 μg/g, Dai et al., 2011a; world low-rank coals, 1.2 μg/g, Ketris and Yudovich, 2009), and is present generally in organic matter and oxide minerals (Eskenazy, 1982; Finkelman, 1995).

Compared to many Chinese and world low-rank coals, the Wulantuga coal is significantly enriched in W (average 115 μg/g). The negative correlation coefficient of W-ash yield (−0.29) and high correlation coefficient of W-Ge (0.95) indicate an organic affinity. Although the correlation coefficient of W-SiO_2 is low (−0.29), a relatively high concentration of W was detected in quartz and chlorite of hydrothermal origin, 1–1.73% with an average of 1.36%, and 1–1.15% with an average of 1.08%, respectively (Table 5).

4.5.3.8. Cesium. The concentration of Cs in the Wulantuga coal varies from 2.67 to 23.45 μg/g and averages 5.29 μg/g, higher than that in Chinese (1.13 μg/g; Dai et al., 2011a) and world low-rank coals (0.98 μg/g; Ketris and Yudovich, 2009).

The mode of Cs occurrence in coal has not been studied in great detail. Cesium can isomorphously substitute for K, so it generally occurs in K-bearing minerals (Swaine, 1990; Tang and Huang, 2004). The Ge-rich coal from the Spetzugli deposit is enriched in Cs (up to 57.2 μg/g), with the Cs being adsorbed by both clay and organic matter (Seredin, 2003b). The high correlation coefficient for Cs-ash (0.78) indicates that the Cs has a dominant inorganic affinity, and those of Cs-K_2O (0.97), Cs –SiO_2 (0.72), and Cs-Al_2O_3 (0.75) indicate that illite is the major carrier of Cs in the Wulantuga coal.

4.5.3.9. Antimony. Antimony has a low abundance in both the Chinese and world low-rank coals (both average 0.84 μg/g). The Sb concentration in the Wulantuga coal is high and greatly varies through the section examined, ranging from 6.0 to 692.5 μg/g with a weighted average of 239.5 μg/g.

Antimony in coal is generally distributed in sulfides (Dai et al., 2006; Swaine, 1990), although some studies have shown that Sb can also be associated with organic matter (Finkelman, 1995). The latter is typical for the high-Ge coal of the Spetzugli deposit, the Sb concentration of which reaches 1175 μg/g and for which the correlation coefficient between Ge and Sb is also very high (0.90; see Seredin, 2003a).

However, the high correlation coefficients of Sb-S_t (0.28) and Sb-Fe_2O_3 (0.32) for the Wulantuga Ge-rich coals indicate that the Sb may occur in pyrite. In addition, the high correlation coefficients of Sb-Hg (0.65), Sb-Tl (0.69), and probably Sb-As (0.32) suggest that Sb, Tl, As, and Hg have a similar source. However, the correlation coefficients of Ge-Sb (0.00) and W-Sb (−0.28) indicate that the element associations Ge-W and Sb-Tl-Hg-As might have been derived from different hydrothermal sources.

4.5.4. Affinity of the elements deduced from correlation of the element concentrations with ash yield

Correlation of the element concentrations with ash yield may provide preliminary information on their organic or inorganic affinity

Table 10
REE concentrations in the Wulantuga coal and their comparison with the Chinese coals and world low-rank coals (elements in μg/g; on whole-coal basis).

Element/Ash	C6-1	C6-2	C6-3	C6-4	C6-5	C6-6	C6-7	C6-8	C6-9	C6-10	C6-11	C6-12	C6-13	WA	China [a]	World [b]	CC [c]	C[d]
Ash	18.6	8.88	2.88	6.48	7.11	7.13	15.9	8.7	12.1	6.75	5.47	8.94	8.03	8.77	nd	nd	nd	1.00
La	9.90	4.14	1.63	2.47	3.97	3.92	8.30	3.91	12.72	2.45	1.94	3.26	2.84	4.78	22.5	10	0.48	0.82
Ce	20.74	8.19	3.33	4.83	7.55	7.55	15.87	8.23	22.80	5.97	4.23	6.90	6.71	9.54	46.7	22	0.43	0.87
Pr	2.56	1.00	0.42	0.57	0.89	0.87	1.77	1.05	2.45	0.86	0.55	0.82	0.85	1.14	6.42	3.5	0.32	0.90
Nd	9.57	3.81	1.76	2.13	3.10	3.09	6.10	4.05	8.56	3.57	2.19	3.09	3.44	4.23	22.3	11	0.38	0.90
Sm	2.02	0.78	0.41	0.43	0.63	0.60	1.17	0.88	1.73	0.74	0.43	0.57	0.79	0.87	4.07	1.9	0.46	0.88
Eu	0.40	0.18	0.09	0.09	0.13	0.11	0.21	0.12	0.18	0.10	0.09	0.10	0.19	0.15	0.84	0.5	0.30	0.88
Gd	1.93	0.86	0.48	0.46	0.61	0.59	1.11	0.86	1.64	0.73	0.43	0.58	0.94	0.88	4.65	2.6	0.34	0.87
Tb	0.27	0.12	0.07	0.06	0.10	0.09	0.16	0.13	0.24	0.10	0.06	0.08	0.14	0.13	0.62	0.32	0.40	0.85
Dy	1.57	0.73	0.44	0.38	0.51	0.50	0.94	0.83	1.51	0.63	0.35	0.49	0.96	0.79	3.74	2	0.39	0.82
Ho	0.29	0.14	0.08	0.07	0.11	0.10	0.18	0.16	0.28	0.13	0.07	0.10	0.20	0.15	0.96	0.5	0.31	0.80
Er	0.85	0.41	0.26	0.22	0.30	0.29	0.53	0.48	0.84	0.40	0.22	0.31	0.62	0.46	1.79	0.85	0.54	0.79
Tm	0.11	0.05	0.03	0.02	0.05	0.04	0.07	0.07	0.11	0.06	0.03	0.04	0.08	0.06	0.64	0.31	0.20	0.80
Yb	0.78	0.35	0.22	0.20	0.29	0.28	0.50	0.45	0.78	0.42	0.20	0.28	0.53	0.42	2.08	1	0.42	0.79
Lu	0.09	0.03	0.01	0.01	0.04	0.02	0.06	0.05	0.09	0.05	0.01	0.02	0.06	0.04	0.38	0.19	0.23	0.80
Y	8.76	4.76	3.06	2.73	2.89	2.84	5.12	4.59	7.73	4.30	2.56	3.86	7.95	4.92	18.2	8.6	0.57	0.72
Sum	59.84	25.55	12.29	14.67	21.17	20.89	42.09	25.86	61.66	20.51	13.36	20.5	26.3	28.56	135.9	65.27	0.44	0.88

nd, no data; [a], Average concentrations of elements in Chinese coals (Dai et al., 2011a); [b], Average concentrations of elements in the world low-rank coals (Ketris and Yudovich, 2009); [c],CC, ratio of concentrations of elements in the Wulantuga coal to the world low-rank coals; C[d], correlation coefficient of REE and ash yield. Sum = REE + Y.

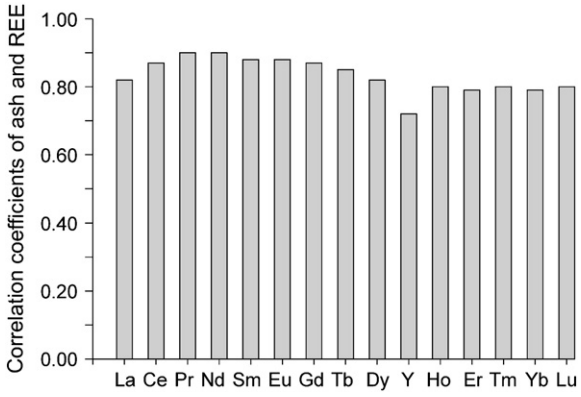

Fig. 25. Correlation coefficients between REE and ash yield.

(Kortenski and Sotirov, 2002), although in some cases the affinity of the elements is not correctly reflected by this indirect method (Dai et al., 2011c; Eskenazy et al., 2010). Five groups (1 to 5) of elements from the present study can be distinguished in terms of their correlation coefficients with ash yield (Table 9).

Group 1 includes MgO, Al_2O_3, SiO_2, K_2O, TiO_2, Li, F, Sc, V, Cr, Cu, Rb, Y, Nb, Ag, Cd, In, Sn, Cs, REE, Hf, Ta, Pb, Bi, Th, and U, which are strongly correlated with ash yield (r_{ash} = 0.7– 1.0). Silicon, Al, and K are major constituents of the aluminosilicate minerals (kaolinite and illite). In addition, quartz is the major carrier of Si in this coal. Other trace elements have relatively high correlation coefficients with both Al_2O_3 and SiO_2, indicating an aluminosilicate affinity.

Group 2 includes elements (P_2O_5, Sr, and Zr) with a lesser but still relatively high inorganic affinity (r = 0.40-0.69; Table 9). Strontium and Zr have high correlation coefficients with P_2O_5 (Table 9), indicating a phosphate affinity.

Group 3 includes CaO (0.34), MnO (0.28), Be (0.37), Ni (0.25), Ba (0.38), which have correlation coefficients with ash yield varying from 0.25 to 0.38. Among these elements, CaO, MnO, and Be have a carbonate affinity, expressed by higher correlation coefficients with CaO (Table 9). Nickel and Ba have a sulfur/sulfate affinity.

Group 4 includes Na_2O, Co, Zn, Ga, Mo, Se, Hg, and Tl. These elements have correlation coefficients with ash yield that range from −0.18 to 0.16, indicating mixed (organic and inorganic) affinity. With the exception of Na_2O, the inorganic proportion of these elements mainly occur in pyrite, because the correlation coefficients of these elements with total sulfur and for each pair of Co, Zn, Ga, Mo, Se, Hg, Tl, are high (Table 9).

Group 5 includes Ge, As, Sb, and W (Table 9). Germanium and a portion of the As, Sb, and W are associated with the organic matter. These elements have negative correlation coefficients with ash yield, indicating an organic affinity. However, portions of the As, Sb, and W are also distributed in pyrite and quartz, respectively, as described above.

4.5.5. Distribution pattern and origin of rare earth elements (REE) and yttrium

The REE + Y concentration in the coal bench samples ranges from 12.3 to 61.7 μg/g (Table 10). The weighted average in the entire section is 28.6 μg/g. This is nearly half of the average REE + Y content in USA coals (62.1 μg/g; see Finkelman, 1993) and world low-rank

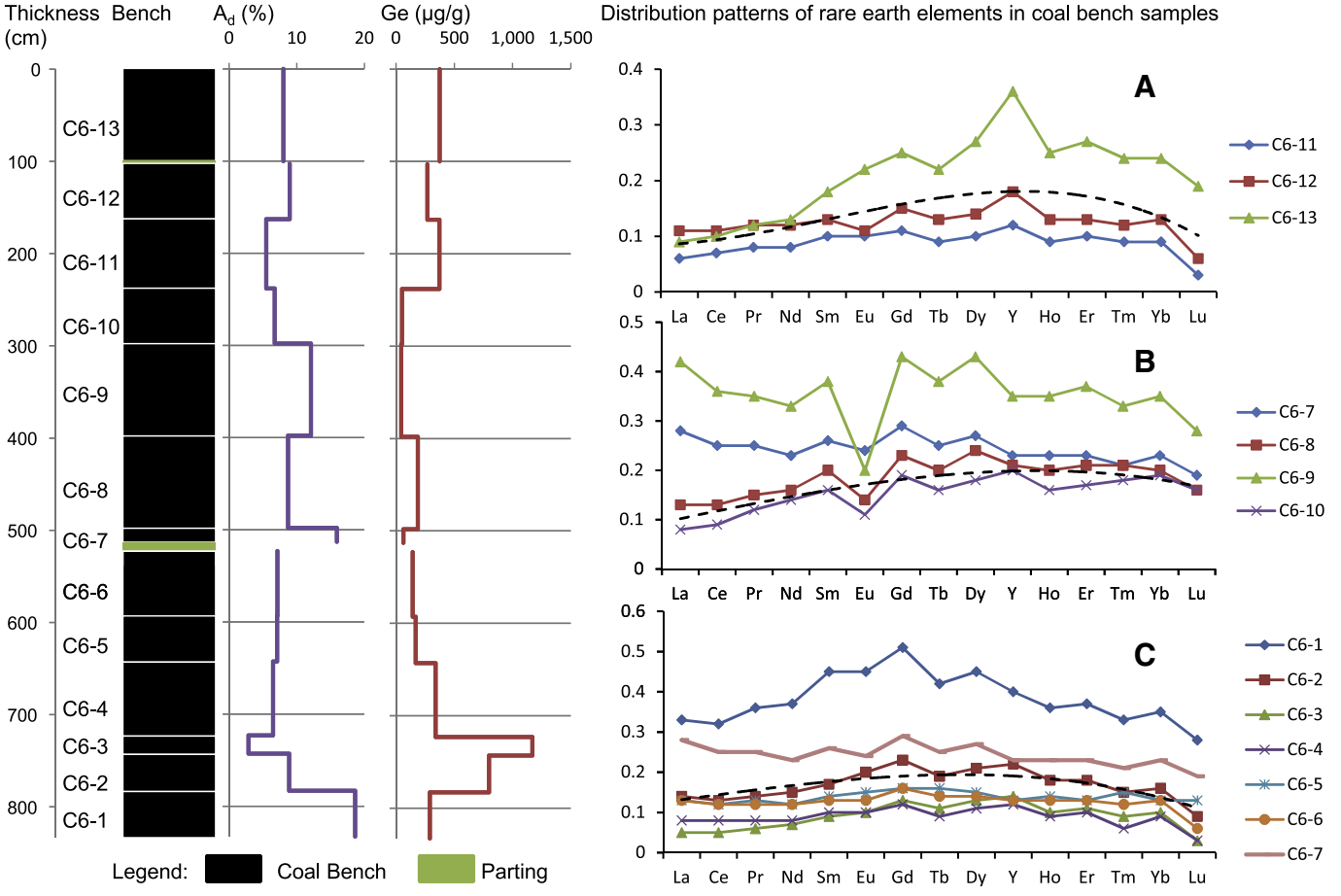

Fig. 26. Ash yield, Ge concentration, and REE distribution pattern in the section of the No. 6 Coal. REE plots are normalized by Upper Continental Crust (UCC) (Taylor and McLennan, 1985). The broken lines are polynomial curves of 3 power approximating average REE plots for samples C6-11–C6-13 (A), C6-8 and 10 (B), C6-1–C6-6 (C).

coals (65.3 μg/g; see Ketris and Yudovich, 2009), and less than a quarter of average concentration of these metals in Chinese coals (135.9 μg/g; Dai et al., 2011a).

The maximum REE + Y concentrations (42.09, 59.83, and 61.66 μg/g, respectively) occur in the coal bench samples with relatively high ash yields (15.9, 18.6, and 12.1%, respectively), and the minimum values (12.3 and 13.4 μg/g, respectively) in the low-ash coal samples (2.9 and 5.5%, respectively). The correlation coefficient between individual REE concentrations and ash yield varies from 0.71 (Y-A_d) to 0.9 (Nd-A_d), showing a slightly higher affinity of LREE to the mineral matter of the coal than that of the HREE and Y (Fig. 25; Table 10). These data support previous conclusions on the close positive correlation of REE concentrations with ash yields and on the major detrital source of the REE elements in the Wulantuga coal (Qi et al., 2007b).

However, the variation of REE distribution patterns through the seam section shows a more complicated relationship between REE and ash yield (Fig. 26). According to the REE distribution patterns, the section in the present study can be divided into three zones: upper (a), middle (b), and lower (c).

The upper zone of the seam, consisting of coal bench samples C6-13 to C6-11, is characterized by similar normalized REE-plots with Y-maxima and relatively high HREE in comparison with LREE (Fig. 27A), showing an H-type distribution pattern (HREE enrichment). The concentrations of REE and Y-maxima decrease downwards in the zone, irrespective of ash yield variation but in accordance with the variation of quartz concentration in the samples.

An H-type REE distribution pattern is normal in coal because many natural solutions enriched in HREE can circulate in coal basins (Seredin, 2001; Seredin and Dai, in press). These solutions include alkaline terrestrial water (Johanneson and Zhou, 1997), some high

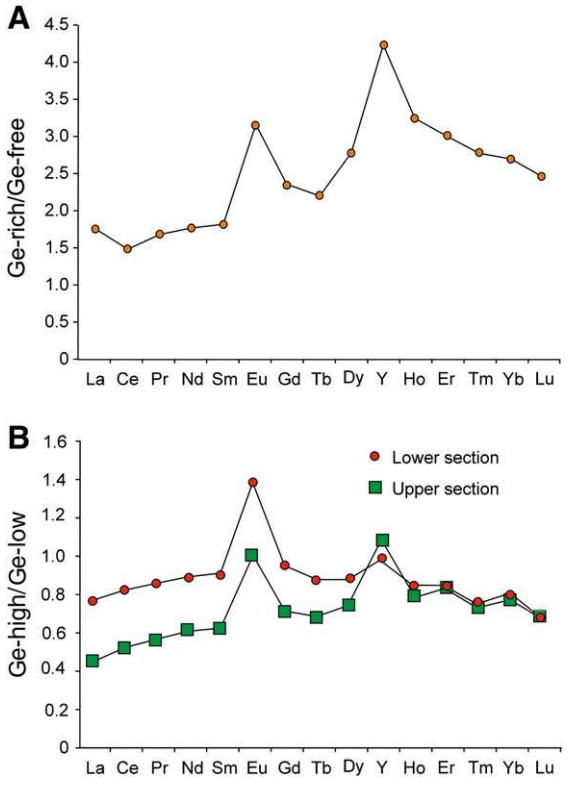

Fig. 27. REE plots for high-Ge coals of Pavlovka (A) and Wulantuga (B) deposits normalized by free- and relatively low-Ge coals. Pavlovka deposit: Ge-rich coals of seam I (drill hole 4), Ge–762 μg/g; Ge-free coals of seam I (open mine), Ge–1 μg/g; data from Seredin (2005).Wulatuga deposit: Ge-high coals of upper section (the weighted average data for samples C6-11–13), Ge–348 μg/g; Ge-high coals of lower section (the weighted average data for samples C6-1–4), Ge–510 μg/g; Ge-low coals (the weighted average data for samples C6-5–10), Ge–115 μg/g.

pCO_2 weakly acid cold mineral water (Shand et al., 2005), some low-temperature (130 °C) alkaline hydrothermal solutions (Michard and Albarède, 1986), and high-temperature (>500 °C) acid volcanogenic fluids (Rybin et al., 2003).

Hydrothermal REE input is more probable in this case because of the occurrence of the abnormally high proportion of quartz of authigenic origin as described above, as well as the high Ge, As, Sb, Hg, and Tl contents of the low-ash coal bench samples in the uppermost part of the seam (Fig. 24).

Coal bench samples C6-10 to C6-7 comprise the middle zone. The REE distribution patterns are different to those in the upper zone of the seam (Fig. 26B).

Eu-minima appear in the REE distribution patterns, and the high-ash coal bench sample (C6-9) displays the lowest Eu content. The REE spectrum with the right-inclined shape (L-type REE distribution) has the typical characteristics of acid magmatic rocks that developed in the vicinity and in the basement of the deposit. The highest kaolinite proportion occurs and the concentrations of Zr and P_2O_5 sharply increase in this sample. It was inferred that the major REE carrier here may be detrital monazite found in the high-ash coal samples of this deposit earlier (Qi et al., 2007b). The low-ash coal bench samples, C6-8 and C6-10, have H-type REE distribution patterns with smaller Eu-minima.

The high-ash coal bench sample C6-7, overlying the parting layer, also has an L-type REE distribution pattern; however, the distribution pattern is more similar to that of shale than that of granite because of the very small Eu-minimum. Apparently, the terrigenous input to this zone was the main source of REE in the relatively high-ash coal bench samples (C6-7 and C6-9) and also influenced the REE geochemistry of the low-ash ones (C6-8 and C6-10).

The REE distribution patterns in the coal bench samples of the lower zone (from C6-1 to C6-6) are characterized by the enrichment of medium REE (M-type REE). The lowermost bench sample C6-1 has the highest REE concentration, which is clearly characterized by an M-type REE plot.

The M-type of REE distribution pattern is not the typical characteristic for rocks but is rather typical for any acid natural water (Johanneson and Zhou, 1997), including acid hydrothermal solutions with especially high REE concentrations (McLennan, 1989).

Participation of hydrothermal solutions in REE accumulation in the lowermost interval of the zone (sample C6-1), where M-type of REE distribution is fixed most accurately, may have produced high concentrations of F, Cs, and K here. The presence of hydrothermal quartz in samples C6-1, C6-2, and C6-3 supports this assumption.

Thus, syngenetic detrital input only influenced the REE distribution patterns in the middle zone of the coal seam. In the upper and lower zones, the enrichment of metals is mainly attributed to the hydrothermal solution input, with REE ions subsequently bound by organic matter. Judging by the low REE concentration in the coals and the different form of the UCC-normalized plots, these solutions had low concentrations of these metals and had unequal chemical compositions. This assumption is supported by the distinctions in chemical and mineral compositions of the upper and lower zones of the seam.

The following stages of the REE accumulation history in the coals can be identified:

(1) Early syngenetic hydrothermal stage: This was coincident with the period of peat accumulation corresponding to the lower zone of the seam. Rare earth elements in this zone could be derived from an ascending acid hydrothermal solution. The source and the composition of the hydrothermal solution was inferred from the M-type REE distribution pattern, and ascending movement identified by the decreasing trend of REE concentration from the bottom to the top of this zone.
(2) Middle syngenetic terrigenous stage: This occurred after formation of the parting layer between C6-6 and C6-7. In this

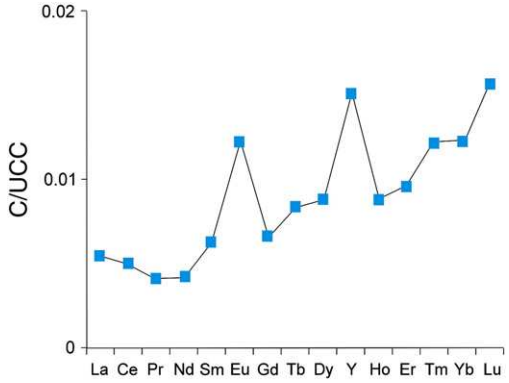

Fig. 28. REE plots for siliceous hydrothermal rocks of Lincang Ge-deposits (constructed according to average data for 10 samples (Hu et al., 2009)). Normalized by UCC.

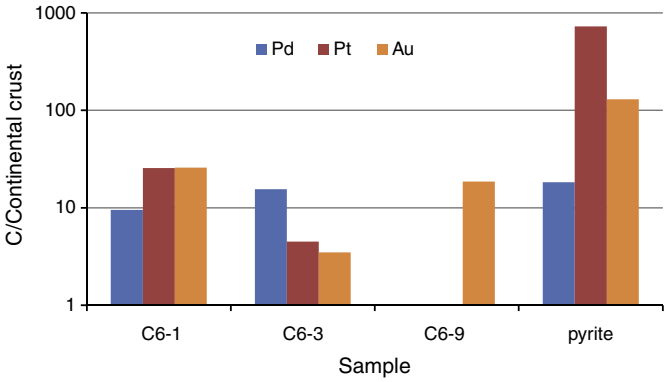

Fig. 29. Concentration coefficients of precious metals in the Wulantuga coal and pyrite samples.

stage, REEs were derived from the detrital minerals of terrigenous origin.

(3) Late diagenetic hydrothermal stage: This possibly began after the accumulation of the overlying sand roof. In this stage, REE arrived in the buried peat through a porous and permeable roof with a new input of hydrothermal solutions. These solutions were enriched in HREE, Y, and SiO_2. Unlike the earlier hydrothermal solutions, the metalliferous hydrothermal solution of this stage was enriched in Sb, Hg, and Tl, along with high Ge, W, and As. Abnormal concentration of all these metals has been found in fossil wood from sandstone at the roof of the seam (Du et al., 2009). These data, and also the considerable thickness of the upper zone, indicate that REE input by hydrothermal solutions occurred after the peat burial but prior to organic matter coalification.

Therefore, REE accumulation in the coals of the studied section of the Wulantuga deposit had a polygenetic and multistage nature, including two syngenetic stages (early hydrothermal and terrigenous) and one diagenetic (late hydrothermal) stage.

Multistage and polygenetic REE accumulation has been proposed earlier for the Ge-bearing coals of the Pavlovka (Spetzugli) deposit, where a syngenetic terrigenous stage and two hydrothermal stages (diagenetic and epigenetic) of REE accumulation have been allocated (Seredin, 2005). Only one of hydrothermal stages (early) was Ge-bearing in the Pavlovka deposit. During the early diagenetic stage, Ge-bearing coals of the Pavlovka deposit were weakly enriched in HREE but significantly enriched in Eu and Y relative to the free-Ge coals of the deposit (Fig. 27A). A similar situation occurred in the Wulantuga deposit (Fig. 27B). Moreover, the similar form of the REE plot is typical for Ge-bearing hydrothermal siliceous rocks, which lie at the contacts with high-Ge coals in the Lincang deposits (Fig. 28). These data showed that the REE composition of Ge-bearing hydrothermal solutions was very similar for all these giant, currently mined Ge-coal deposits.

4.5.6. Au and platinum group elements (PGE)

Table 11 lists the concentrations of Au and PGEs in the coal ash, pyrite, and the estimated values for the coals, as well as the comparison with their concentrations in the continental crust.

All the analyzed high-Ge coal samples are abnormally enriched in precious metals in comparison with the continental crust (Table 11, Fig. 29). The concentration coefficients of Au, Pt, and Pd in the coal, calculated from their concentration in the LTAs, are in the range of 3.5–25.8, < 4–25.5, and<2.5–15.5, respectively. The concentrations of Pd and Pt are also much higher than those of the sedimentary cover of the North China Platform, which have been estimated as 0.35 and 0.25 ng/g, respectively (Chi and Yan, 2006).

The concentrations of precious metals and their relations with ash yield vary considerably in the different coal bench samples through the section. The maximum Au and Pt concentrations occur together in the lowermost bench sample (C6-1), which has a relatively high ash yield (Table 1). The maximum Pd concentration was found in the low-ash (8.71%), but high-Ge (1170 μg/g), 20-cm thick coal bench sample C6-3. The relationship between the concentrations of Au and PGEs and the ash yields accords with published data (Lakatos et al., 1997; Varshal et al., 2000) concerning the higher organic affinity of Pd in comparison with other precious metals.

The concentrations of PGEs in the central portion of bench C6-9, which has a low-Ge concentration (45 μg/g), are below the detection limit. However, the Au concentration in this bench sample is abnormally high.

Table 11
Precious metal concentrations (ng/g) in low-temperature and high-temperature ashes of the coal samples, pyrite, and estimated values for the coals, as well as the comparison with their concentration in continental crust.

Samples	Material	Mass (g)	Ash (%)	Pd	Pt	Au	Sum
Measured values							
C6-1*	HTA	1.75	23.4	7.8	31.6	113.2	152.6
C6-1*	LTA	1.0	29.53	12.8	34.4	219.1	266.3
C6-3	LTA	0.7	8.71	71.0	21.0	100.0	192.0
C6-9	LTA	1.0	19.87	<5	<8	234.0	>234.0
Prt*	Pyrite	2.0		7.3	290.0	324.4	621.6
Estimated values							
C6-1	Coal based on HTA	7.5	23.4	1.8	7.4	26.5	35.7
C6-1	Coal based on LTA	3.4	29.53	3.8	10.2	64.6	78.5
C6-3	Coal based on LTA	8.2	8.71	6.2	1.8	8.71	16.7
C6-9	Coal based on LTA	5.3	19.87	<1.0	<1.6	46.5	>46.5
Continental crust**				0.4	0.4	2.5	3.3

Note. *, average data of two parallel analyses; The concentrations of Au-PGEs in LTHs, HTA, and pyrite are determined values, and those of coal samples are estimated based on HTA or LTAs; **, data from Wedepohl (1995).

The highest concentrations of precious metals occur in the pyrite and are 18 (Pd), 130 (Au), and 725 (Pt) times higher than those of the continental crust.

It is inferred that precious metals may be present in the sulfides as isomorphic impurities, because no discrete minerals of the precious metals were observed under SEM-EDX. The significant enrichment of Au and especially Pt in the pyrite indicates that the pyrite probably is the basic carrier of Pt and some portion of the Au in the coal. However, a certain portion of precious metals may be organically (halogen-organic) bound in coal bench sample C6-1. The higher precious metal concentrations in the LTA than the HTA of sample C6-1 can probably be attributed to the loss (maximum for Au, minimum for Pt) of these metals during high-temperature ashing, as some of precious-metal organic compounds, for example, carbonyls and halogen-carbonyls, are volatile at a relatively low (>200 °C) temperatures (Mitkin et al., 2000, and references in this work).

Thus, the previous conclusion on abnormal concentrations of Ir and Au in the Wulantuga coal (Zhuang et al., 2006) has been confirmed by this investigation. The new data in the present study provided the first understanding of Pt and Pd concentration in the Wulantuga coals and showed that high Au and PGE concentrations not only typically occur at the top of No. 6 coal seam, but are also found at the lower part. The high Au + PGE sum in pyrite (0.6 μg/g) and the coal ash (0.15-0.25 μg/g) suggests a need for further study of these coals as possible source for precious metals as by-products.

5. Conclusions

The Ge-rich No. 6 Coal in the Wulantuga Ge deposit is a low-rank ($R_{o,max}$ = 0.45%; V_{daf} = 36.32%), low-ash (8.77%), and medium- to high-sulfur ($S_{t,d}$ = 1.07-2.40%) coal. The total inertinite content in most coal benches is high (52.5% on average); fusinite (33%) and semifusinite dominate. The huminite group (46.8% on average) comprises mainly textinite. Palynologically, the coal is characterized by an assemblage of bryophytes, pteridophytes, and gymnosperms that, together, indicate deposition under warm, humid, but seasonally dry conditions. High inertinite counts also support seasonal dryness. The recovered assemblage is consistent with a lower Cretaceous age, likely Aptian as suggested by Sha (2007). The taxa recovered indicate freshwater conditions during peat accumulation.

The mineral matter in the Ge-rich coal mainly consists of quartz, kaolinite, illite (and/or illite/smectite), gypsum, pyrite, and traces of rutile and anatase. Bassanite was observed with a varying percentage in the low temperature ash and is believed to be derived both from dehydration of gypsum in the raw coals and as an artifact of the low-temperature ashing process. A large proportion of quartz occurs as cell-fillings and fine-grained particles in the organic matter, indicating an authigenic origin. The syngenetic pyrite was derived from sulfate-rich hydrothermal fluids rather than seawater.

Elements with elevated concentrations in the Wulantuga coal include Be (25.7 μg/g), F (336 μg/g), Ge (273 μg/g), As (499 μg/g), Sb (240 μg/g), Cs (5.29 μg/g), W (115 μg/g), Hg (3.165 μg/g), and Tl (3.15 μg/g). In accordance with studies of other researchers, Ge is organically associated and derived from the adjacent granitoids via hydrothermal circulation.

In contrast to elevated Be contents in other coals generally being associated with the organic matter, Be in the Wulantuga coal is mainly associated with Ca- and Mn-bearing carbonate minerals and to a lesser extent with clay minerals. A large proportion of F also occurs in the clay minerals (kaolinite and illite). The elevated Tl, Hg, As, and Sb have the same hydrothermal source and are predominantly distributed in pyrite. Both the organic matter and the authigenic quartz are the carriers of elevated W in the coal. Cesium mainly occurs in illite.

According to the REE distribution patterns, the coal seam section can be divided into three zones. The REEs in the lower zone (C6-1 to C6-6) are characterized by medium REE enrichment (M-type), where syngenetic hydrothermal solutions were precipitated. The middle zone (C6-7 to C6-10) has an L-type REE distribution, and terrigenous input was the major source of REEs. The upper zone, consisting of C6-11 and C6-13, is characterized by an H-type REE distribution, which is attributed to a late hydrothermal solution input.

The Wulantuga coal is significantly enriched in Au, Pt, and Pd (concentration coefficients 3.5–25.8, < 4–25.5, and < 2.5–15.5, respectively). Their concentrations in pyrite are 130 (Au), 725 (Pt), and 18 (Pd) times higher than those of the continental crust. Platinum mainly occurs in pyrite, whereas a certain portion of precious metals, especially Pd and Au, may be organically bound in the coal.

Acknowledgements

This research was supported by the cooperative project between National Natural Science Foundation of China and Russian Foundation of Basic Research (nos. 10-05-91160 and 41011120095), National Natural Science Foundation of China (nos. 40930420 and 40725008), the Presidium of the Russian Academy of Sciences (program 23, project 1.1.1), and the Fundamental Research Funds for the Central Universities (no. 2011YM02). Special thanks are given to Mr. Guojun Wei for his assistance during field work and sample collection. The authors are grateful to Mr. Yiping Zhou and Dr. Yaofa Jiang for their support and to V. Sychkova, Yu. Shazzo, and D. Petrenko for precious metal determinations. The two anonymous reviews and editor Ralf Littke are highly appreciated for their careful and constructive comments for the manuscript.

References

ASTM D2797-04, 2005. Annual Book of ASTM Standards. Gaseous Fuels; Coal and Coke, vol. 05.06. Practice for Preparing Coal Samples for Microscopical Analysis by Reflected Light.

ASTM D2798-05, 2005. Annual Book of ASTM Standards. Gaseous Fuels; Coal and Coke, vol. 05.06. Test Method for Microscopical Determination of the Vitrinite Reflectance of Coal.

ASTM D3173-03, 2005. Annual Book of ASTM Standards. Gaseous Fuels; Coal and Coke, vol. 05.06. Test Method for Moisture in the Analysis Sample of Coal and Coke.

ASTM D3174-04, 2005. Annual Book of ASTM Standards. Gaseous Fuels; Coal and Coke, vol. 05.06. Test Method for Ash in the Analysis Sample of Coal and Coke from Coal.

ASTM D3175-02, 2005. Annual Book of ASTM Standards. Gaseous Fuels; Coal and Coke, vol. 05.06. Test Method for Volatile Matter in the Analysis Sample of Coal and Coke.

ASTM D3177-02, 2005. Annual Book of ASTM Standards. Gaseous Fuels; Coal and Coke, vol. 05.06. Test Methods for Total Sulfur in the Analysis Sample of Coal and Coke.

Belkin, H.E., Zheng, B.S., Zhou, D.X., 1997. Preliminary results on the geochemistry and mineralogy of arsenic in mineralized coals from endemic arsenosis area in Guizhou Province, PR China. 14th Internat. Ann. Pittsburgh Coal Conf. and Workshop Proceedings, pp. 1–20. CD-ROM.

Belkin, H.E., Tewalt, S.J., Hower, J.C., Stucker, J.D., O'Keefe, J.M.K., 2009. Geochemistry and petrology of selected coal samples from Sumatra, Kalimantan, Sulawesi, and Papua, Indonesia. International Journal of Coal Geology 77, 260–268.

Belkin, H.E., Tewalt, S.J., Hower, J.C., Stucker, J.D., O'Keefe, J.M.K., Tatu, C.A., Buta, G., 2010. Geochemistry and petrography of Oligocene bituminous coals from the Jiu Valley, Petrosani basin (southern Carpathian Mountains), Romania. International Journal of Coal Geology 82, 68–80.

Boctor, N.Z., Kullerud, G., Sweany, J.L., 1976. Sulfide minerals in Seelyville Coal III, Chinook Mine, Indiana. Mineral Deposita 11, 249–266.

Bouška, V., Pešek, J., Sýkorová, I., 2000. Probable modes of occurrence of chemical elements in coal. Acta Montana Serie B, Fuel, Carbon, Mineral Processing, Praha 117, 53–90.

Brownfield, M.E., Affolter, R.H., Cathcart, J.D., Johnson, S.Y., Brownfield, I.K., Rice, C.A., Zielinski, R.A., 2005. Geologic setting and characterization of coal and the modes of occurrence of selected elements from the Franklin coal zone, Puget Group, John Henry No. 1 mine, King County, Washington. International Journal of Coal Geology 63, 247–275.

Chi, Q.H., Yan, M.C., 2006. Platinum-group element abundances in crust, rocks and sediments. Geochimica 35, 461–471 (in Chinese with English abstract).

Coleman, S.L., Bragg, L.J., 1990. Distribution and mode of occurrence of arsenic in coal. In: Chyi, L.L., Chou, C.-L. (Eds.), Recent Advances in Coal Geochemistry: Geol. Soc. Am., Spec. Pap., vol. 248, pp. 13–26.

Cui, X., Li, J., 1991. The Late Mesozoic stratigraphy and palaeontology of the Erlian Basin Group in Inner Mongolia, China. Geoscience, the Journal of the Graduate School, China University of Geosciences 5, 397–408 (In Chinese with English Abstract).

Cui, X., Li, J., 1993. Late Mesozoic basin types and their coal accumulation characteristics of Erlian basins in Inner Mongolia. Geoscience, the Journal of the Graduate

School, China University of Geosciences 7, 479–484 (In Chinese with English Abstract).
Dai, S., Zeng, R., Sun, Y., 2006. Enrichment of arsenic, antimony, mercury, and thallium in a late Permian anthracite from Xingren, Guizhou, southwest China. International Journal of Coal Geology 66, 217–226.
Dai, S., Tian, L., Chou, C.-L., Zhou, Y., Zhang, M., Zhao, L., Wang, J., Yang, Z., Cao, H., Ren, D., 2008. Mineralogical and compositional characteristics of Late Permian coals from an area of high lung cancer rate in Xuan Wei, Yunnan, China: occurrence and origin of quartz and chamosite. International Journal of Coal Geology 76, 318–327.
Dai, S., Ren, D., Chou, C.-L., Finkelman, R.B., Seredin, V.V., Zhou, Y., 2011a. Geochemistry of trace elements in Chinese coals: A review of abundances, genetic types, impacts on human health, and industrial utilization. International Journal of Coal Geology. doi:10.1016/j.coal.2011.02.003.
Dai, S., Wang, X., Zhou, Y., Hower, J.C., Li, D., Chen, W., Zhu, X., 2011b. Chemical and mineralogical compositions of silicic, mafic, and alkali tonsteins in the late Permian coals from the Songzao Coalfield, Chongqing, Southwest China. Chemical Geology 282, 29–44.
Dai, S., Zou, J., Jiang, Y., Ward, C.R., Wang, X., Li, T., Xue, W., Liu, S., Tian, H., Sun, X., Zhou, D., 2011c. Mineralogical and geochemical compositions of the Pennsylvanian coal in the Adaohai Mine, Daqingshan Coalfield, Inner Mongolia, China: Modes of occurrence and origin of diaspore, gorceixite, and ammonian illite. International Journal of Coal Geology. doi:10.1016/j.coal.2011.06.010.
Ding, Z., Zheng, B., Zhang, J., Long, J., Belkin, H.E., Finkelman, R.B., Zhao, F., Chen, C., Zhou, D., Zhou, Y., 2001. Geological and geochemical characteristics of high arsenic coals from endemic arsenosis areas in southwestern Guizhou Province, China. Applied Geochemistry 16, 1353–1360.
Du, G., Tang, D.Z., Wu, W., Sun, P.C., Bai, Y.L., Xuan, Y.Q., Huang, G.J., 2003. Preliminary discussion on genetic geochemistry of paragenetic germanium deposit in Shenli Coalfield, Inner Mongolia. Geoscience 17, 453–458 (in Chinese with English abstract).
Du, G., Tang, D.Z., Wu, W., Sun, P.C., Bai, Y.L., Yang, W.B., Xuan, Y.Q., Zhang, L.C., 2004. Research on grade variation regularity of paragenetic germanium deposit along uprightness in Shengli Coalfield, Inner Mongolia. Coal Geology & Exploration 32 (1), 1–4 (in Chinese with English abstract).
Du, G., Zhuang, X., Querol, X., Izquierdo, M., Alastuey, A., Moreno, T., Font, O., 2009. Ge distribution in the Wulantuga high-germanium coal deposit in the Shengli coalfield, Inner Mongolia, northeastern China. International Journal of Coal Geology 78, 16–26.
Eskenazy, G.M., 1982. The geochemistry of tungsten in Bulgarian coals. International Journal of Coal Geology 2, 99–111.
Eskenazy, G.M., 1995. Geochemistry of arsenic and antimony in Bulgarian coals. Chemical Geology 119, 239–254.
Eskenazy, G.M., 2006. Geochemistry of beryllium in Bulgarian coals. International Journal of Coal Geology 66, 305–315.
Eskenazy, G.M., Valceva, S.P., 2003. Geochemistry of beryllium in the Mariza-east lignite deposit (Bulgaria). International Journal of Coal Geology 55, 47–58.
Eskenazy, G., Finkelman, R.B., Chattarjee, S., 2010. Some considerations concerning the use of correlation coefficients and cluster analysis in interpreting coal geochemistry data. International Journal of Coal Geology 83, 491–493.
Finkelman, R.B., 1993. Trace and minor elements in coal. In: Engel, M.H., Masko, S.A. (Eds.), Organic Geochemistry. Plenum Press, New York, pp. 593–607.
Finkelman, R.B., 1995. Modes of occurrence of environmentally sensitive trace elements in coal. In: Swaine, D.J., Goodarzi, F. (Eds.), Environmental Aspects of Trace Elements in Coal. Kluwer Academic Publishing, Dordrecht, pp. 24–50.
Finkelman, R.B., Brown Jr., R.D., 1991. Coal as host and as an indicator of mineral resources. In: Peters, D.C. (Ed.), Geology in Coal Resource Utilization. Techbooks, Fairfax, Virginia, pp. 471–481.
Frazer, F.W., Belcher, C.B., 1973. Quantitative determination of the mineral matter content of coal by a radio-frequency oxidation technique. Fuel 52, 41–46.
GB/T 15224. 2–2004 (National Standard of P.R. China), 2004. Classification for Quality of Coal.Part 2: Sulfur content. (in Chinese).
GB/T 15224.1-2004 (National Standard of P.R. China), 2004. Classification for Quality of Coal. Part 1: Ash yield. (in Chinese).
GB/T 4633–1997 (National Standard of P.R. China), 1997. Determination of fluorine in coal. (in Chinese).
GB/T 482–2008 (National Standard of P.R. China), 2008. Sampling of Coal in Seam. (in Chinese).
Godbeer, W.C., Swaine, D.J., 1987. Fluorine in Australian coals. Fuel 66, 794–798.
Guo, Y., Bustin, R.M., 1998. FTIR spectroscopy and reflectance of modern charcoals and fungal decayed woods: implications for studies of inertinite in coals. International Journal of Coal Geology 37, 29–53.
Han, D., Ren, D., Wang, Y., Jin, K., Mao, H., Qin, Y., 1996. Coal Petrology of China. Publishing House of China University of Mining and Technology, Xuzhou, p. 599 (in Chinese with English abstract).
Hower, J.C., Robertson, J.D., 2003. Clausthalite in coal. International Journal of Coal Geology 53, 219–225.
Hower, J.C., Ruppert, L.F., 2011. Splint coals of the Central Appalachians: Petrographic and geochemical facies of the Peach Orchard No. 3 Split coal bed, southern Magoffin County, Kentucky. International Journal of Coal Geology 85, 268–273.
Hower, J.C., Robertson, J.D., Wong, A.S., Eble, C.F., Ruppert, L.F., 1997. Arsenic and lead concentrations in the Pond Creek and Fire Clay coal beds, Eastern Kentucky coal field. Applied Geochemistry 12, 281–289.
Hower, J.C., Eble, C.F., Quick, J.C., 2005a. Mercury in Eastern Kentucky coals: geologic aspects and possible reduction strategies. International Journal of Coal Geology 62, 223–236.
Hower, J.C., Ruppert, L.F., Eble, C.F., Clark, W.L., 2005b. Geochemistry, petrology, and palynology of the Pond Creek coal bed, northern Pike and southern Martin counties, Kentucky. International Journal of Coal Geology 62, 167–181.
Hower, J.C., Campbell, J.L., Teesdale, W.J., Nejedly, Z., Robertson, J.D., 2008. Scanning proton microprobe analysis of mercury and other trace elements in Fe-sulfides from a Kentucky coal. International Journal of Coal Geology 75, 88–92.
Hower, J.C., O'Keefe, J.M.K., Watt, M.A., Pratt, T.J., Eble, C.F., Stucker, J.D., Richardson, A.R., Kostova, I.J., 2009. Notes on the origin of inertinite macerals in coals: Observations on the importance of fungi in the origin of macrinite. International Journal of Coal Geology 80, 135–143.
Hower, J.C., O'Keefe, J.M.K., Volk, T.J., Watt, M.A., 2010. Funginite-resinite associations in coal. International Journal of Coal Geology 83, 64–72.
Hower, J.C., O'Keefe, J.M.K., Eble, C.F., Raymond, A., Valentim, B., Volk, T.J., Richardson, A.R., Satterwhite, A.B., Hatch, R.S., Stucker, J.D., Watt, M.A., 2011a. Notes on the origin of inertinite macerals in coal: Evidence for fungal and arthropod transformations of degraded macerals. International Journal of Coal Geology 86, 231–240.
Hower, J.C., O'Keefe, J.M.K., Eble, C.F., Volk, T.J., Richardson, A.R., Satterwhite, A.B., Hatch, R.S., Kostova, I.J., 2011b. Notes on the origin of inertinite macerals in coal: Funginite associations with cutinite and suberinite. International Journal of Coal Geology 85, 186–190.
Hu, R., Qi, H., Bi, X., Su, W., Peng, J., 2006. Geology and geochemistry of the Lincang superlarge Germanium deposit hosted in coal seams, Yunnan, China. Geochimica et Cosmochimica Acta 70 (Suppl), A269.
Hu, R., Qi, H., Zhou, M., Su, W., Bi, X., Peng, J., Zhong, H., 2009. Geological and geochemical constraints on the origin of the giant Lincang coal seam-hosted germanium deposit, Yunnan, SW China: A review. Ore Geology Reviews 36, 221–234.
Huang, W., Wan, H., Du, G., Sun, L., Ma, Y., Tang, X., Wu, W., Qin, S., 2008. Research on element geochemical characteristics of coal-Ge deposit in Shengli Coalfield, Inner Mongolia, China. Earth Science Frontiers 15, 56–64.
Huggins, F.E., Huffman, G., 1996. Modes of occurrence of trace elements in coal from XAFS spectroscopy. International Journal of Coal Geology 32, 31–53.
International Commission for Coal and Organic Petrology (ICCP), 2001. The new inertinite classification (ICCP System 1994). Fuel 80, 459–471.
Johanneson, K.J., Zhou, X., 1997. Geochemistry of the rare earth element in natural terrestrial waters: A review of what is currently known. Chinese Journal of Geochemistry 16, 20–42.
Kemezys, M., Taylor, G.H., 1964. Occurrence and distribution of minerals in some Australian coals. Journal of the Institute of Fuel 37, 389–397.
Ketris, M.P., Yudovich, Ya.E., 2009. Estimations of Clarkes for Carbonaceous biolithes: World average for trace element contents in black shales and coals. International Journal of Coal Geology 78, 135–148.
Kolker, A., Finkelman, R.B., 1998. Potentially hazardous elements in coal: modes of occurrence and summary of concentration data for coal components. Coal Preparation 19, 133–157.
Kortenski, J., Kostova, I., 1996. Occurrence and morphology of pyrite in Bulgarian coals. International Journal of Coal Geology 29, 273–290.
Kortenski, J., Sotirov, A., 2002. Trace and major element content and distribution in Neogene lignite from the Sofia basin. International Journal of Coal Geology 52, 63–82.
Koukouzas, N., Ward, C.R., Li, Z., 2010. Mineralogy of lignites and associated strata in the Mavropigi field of the Ptolemais Basin, northern Greece. International Journal of Coal Geology 81, 182–190.
Lakatos, J., Brown, S.D., Snape, C.E., 1997. Unexpectedly High Uptake of Palladium by Bituminous Coals. Proceedings of ICCS'97, Essen, DGMK, 1, pp. 247–250.
Li, J., Batten, D.J., 2004. Early Cretaceous palynofloras from the Tanggula Mountains of the northern Qinghai-Xizang (Tibet) Plateau, China. Cretaceous Research 25, 531–542.
Li, W., Liu, Z., 1994. The Cretaceous palynofloras and their bearing on stratigraphic correlation in China. Cretaceous Research 15, 333–365.
Li, J., Zhuang, X., Querol, X., 2011. Trace element affinities in two high-Ge coals from China. Fuel 90, 240–247.
Liu, Q., Zhang, P., 1997. Compositions and Mechanism of Kaolin in the Late Paleozoic Coal-bearing Strata of North China. Ocean Press, Beijing, pp. 24–38 (in Chinese).
McIntyre, N.S., 1985. Study of elemental distributions with discrete coal maceral, use of secondary ion mass spectrometry and X-ray photoelectron spectroscopy. Fuel 64, 1705–1711.
McLennan, S.M., 1989. Rare Earth Elements in Sedimentary Rocks; Influence of Provenance and Sedimentary Processes. Reviews in Mineralogy and Geochemistry 21, 169–200.
Michard, A., Albarède, F., 1986. The REE content of some hydrothermal fluids. Chemical Geology 55, 51–60.
Minkin, J.A., Finkelman, R.B., Thompson, C.L., Chao, E.C.T., Ruppert, L.F., Blank, H., Cecil, C.B., 1984. Microcharacterization of arsenic- and selenium-bearing pyrite in Upper Freeport coal, Indiana County, Pennsylvania. Scanning Electron Microscopy 4, 1515–1524.
Mitkin, V.N., Galizky, A.A., Korda, T.M., 2000. Some observations on the determination of gold and the platinum-group elements in black shales. Geostandards Newsletter 24, 227–240.
Nichols, D.J., Matsukawa, M., Ito, M., 2006. Palynology and age of some Cretaceous nonmarine deposits in Mongolia and China. Cretaceous Research 27, 241–251.
O'Keefe, J.M.K., 2008. Paleogene Mirelands of the Upper Mississippi Embayment, Western Kentucky. Unpublished PhD thesis. University of Kentucky, Lexington, KY, 2287 pp.
O'Keefe, J.M.K., Eble, C.F., in review. A comparison of HF-based and non-HF-based Palynology processing techniques in clay-rich samples from the Claiborne Group, upper Mississippi Embayment, United States. Palynology, submitted.
O'Keefe, J.M.K., Hower, J.C., 2011. Revisiting Coos Bay, Oregon: A re-examination of funginite-huminite relationships in Eocene subbituminous coals. International Journal of Coal Geology 85, 34–42.

O'Keefe, J.M.K., Hower, J.C., Hatch, R., Bartley, R., Bartley, S., 2011. Fungal forms in Miocene Eel River coals: extraction across a rank suite. Abstracts of the 2011 AASP annual meeting: Palynology, 35.
Pavlov, A.V., 1966. Composition of coal ash in some regions of the West Svalboard Uchen. Zap. NIIGA. [Proc. Arctic Geology Sci.-resear. Inst.] Regional. Geol. 8, 128–136.
Prager, A., Barthelmes, A., Theuerkauf, M., Joosten, H., 2006. Non-pollen palynomorphs from modern Alder cars and their potential for interpreting microfossil data from peat. Review of Palaeobotany and Palynology 14, 7–31.
Qi, L., Gao, J., 2008. Revisiting platinum group elements of Late Permian coals from western Guizhou Province, SW China. International Journal of Coal Geology 75, 189–193.
Qi, H., Hu, R., Su, W., Qi, L., Feng, J., 2004. Continental hydrothermal sedimentary siliceous rock and genesis of superlarge germanium (Ge) deposit hosted in coal: a study from the Lincang Ge deposit, Yunnan, China. Sciences in China Series D: Earth Sciences 47, 973–984.
Qi, H., Hu, R., Zhang, Q., 2007a. Concentration and distribution of trace elements in lignite from the Shengli Coalfield, Inner Mongolia, China: Implications on origin of the associated Wulantuga Germanium Deposit. International Journal of Coal Geology 71, 129–152.
Qi, H., Hu, R., Zhang, Q., 2007b. REE Geochemistry of the Cretaceous lignite from Wulantuga Germanium Deposit, Inner Mongolia, Northeastern China. International Journal of Coal Geology 71, 329–344.
Qing, S.L., 2001. Preservative principals of germanium deposit in Shengli Coal-field of Inner Mongolia and prospecting direction. Coal Geology of China 13 (3), 18–19 (in Chinese with English abstract).
Rao, C.P., Gluskoter, H.J., 1973. Occurrence and distribution of minerals in Illinois coals. Illinois State Geological Survey Circular, 476, p. 56.
Ren, D.Y., 1996. Mineral matters in coal. In: Han, D.X. (Ed.), Coal Petrology of China. Publishing House of China University of Mining and Technology, Xuzhou, pp. 67–77 (in Chinese with English abstract).
Rietveld, H.M., 1969. A profile refinement method for nuclear and magnetic structures. Journal of Applied Crystallography 2, 65–71.
Ruppert, L.F., Cecil, C.B., Stanton, R.W., 1985. Authigenic quartz in the Upper Freeport coal bed, west-central Pennsylvania. Journal of Sedimentary Petrology 55, 334–339.
Ruppert, L.F., Stanton, R.W., Cecil, C.B., Eble, C.F., Dulong, F.T., 1991. Effects of detrital influx in the Pennsylvanian Upper Freeport peat swamp. International Journal of Coal Geology 17, 95–116.
Ruppert, L.F., Minkin, J.A., McGee, J.J., Cecil, C.B., 1992. An unusual occurrence of arsenic-bearing pyrite in the Upper Freeport coal bed, west-central Pennsylvania. Energy & Fuels 6, 120–125.
Rybin, A.V., Gur'yanov, V.B., Chibisova, M.V., Zharkov, R.V., 2003. Rhenium Exploration Prospects on Sakhalin and the Kuril Islands. Geodynamics, Magmatism, and Mineralogeny of the North Pacific Ocean. Magadan, Vol. 3, pp. 180–183 (in Russian).
Scott, A.C., 1989. Observations on the nature and origin of fusain. International Journal of Coal Geology 12, 443–475.
Scott, A.C., 2000. The pre-quaternary history of fire. Palaeogeography, Palaeoclimatology, Palaeoecology 164, 281–329.
Scott, A.C., 2002. Coal petrology and the origin of coal macerals: A way ahead? International Journal of Coal Geology 50, 119–134.
Scott, A.C., Glasspool, I.J., 2005. Charcoal reflectance as a proxy for the emplacement temperature of pyroclastic flow deposits. Geology 33, 589–592.
Scott, A.C., Glasspool, I.J., 2007. Observations and experiments on the origin and formation of inertinite group macerals. International Journal of Coal Geology 70, 53–66.
Scott, A.C., Jones, T.P., 1994. The nature and influence of fire in Carboniferous ecosystems. Palaeogeography, Palaeoclimatology, Palaeoecology 106, 91–112.
Scott, A.C., Cripps, J.A., Collinson, M.E., Nichols, G.J., 2000. The taphonomy of charcoal following a recent heathland fire and some implications for the interpretation of fossil charcoal deposits. Palaeogeography, Palaeoclimatology, Palaeoecology 164, 1–31.
Seredin, V.V., 2001. Major regularities of the REE distribution in coal. Dokl. Earth Sci. 377, 250–253.
Seredin, V.V., 2003a. Anomalous trace elements contents in the Spetsugli germanium deposit (Pavlovka brown coal deposit) southern Primorye: communication 1. Antimony. Lithology and Mineral Resources 38, 154–161.
Seredin, V.V., 2003b. Anomalous concentrations of trace elements in the Spetsugli Germanium deposits (Pavlovka Brown Coal Deposit, Southern Primorye): communication 2. Rubidium and Cesium. Lithology and Mineral Resources 38, 233–241.
Seredin, V.V., 2004. The Au-PGE mineralization at the Pavlovsk Brown Coal Deposit, Primorye. Geology of Ore Deposits 46, 36–63.
Seredin, V.V., 2005. Rare earth elements in germanium-bearing coal seams of the Spetsugli deposit (Primor'e region, Russia). Geology of Ore Deposits 47, 238–255.
Seredin, V.V., 2007. Distribution and formation conditions of noble metal mineralization in coal-bearing basins. Geology of Ore Deposits 49, 1–30.
Seredin, V.V., Dai, S., in press. Coal deposits as a potential alternative source for lanthanides and yttrium. International Journal of Coal Geology. doi:10.1016/j.coal.2011.11.001.
Seredin, V.V., Finkelman, R.B., 2008. Metalliferous coals: A review of the main genetic and geochemical types. International Journal of Coal Geology 76, 253–289.
Seredin, V.V., Shpirt, M.Y., 1995. Metalliferous coals: a new potential source of valuable trace elements as by-products. Coal Science (Proceedings ICCS '95), Pajares, Tascon. Elsevier Science B. V., pp. 1649–1652. II.
Sha, J., 2007. Cretaceous stratigraphy of northeast China: non-marine and marine correlation. Cretaceous Research 28, 146–170.
Shand, P., Johannesson, K.H., Chudaev, O., Chudaeva, V., Edmunds, W.M., 2005. Rare Earth Element Contents of High pCO2 Groundwaters of Primorye, Russia: Mineral Stability and Complexation Controls. In: Johannesson, K.H. (Ed.), Rare Earth Elements in Groundwater Flow System. Springer, The Netherlands, pp. 161–186.
Siavalas, G., Linou, M., Chatziapostolou, A., Kalaitzidis, S., Papaefthymiou, H., Christanis, K., 2009. Palaeoenvironment of Seam I in the Marathousa Lignite Mine, Megalopolis Basin (Southern Greece). International Journal of Coal Geology 78, 233–248.
Swaine, D.J., 1990. Trace Elements in Coal. Butterworths, London. 278 pp.
Sýkorová, I., Pickel, W., Christanis, K., Wolf, M., Taylor, G.H., Flores, D., 2005. Classification of huminite—ICCP System 1994. International Journal of Coal Geology 62, 85–106.
Tang, X., Huang, W., 2004. Trace Elements in Chinese coals. The Commercial Press, Beijing, pp. 6–11. 24–25, (in Chinese).
Taylor, J.C., 1991. Computer programs for standardless quantitative analysis of minerals using the full powder diffraction profile. Powder Diffraction 6, 2–9.
Taylor, S.R., McLennan, S.M., 1985. The continental crust: its composition and evolution. Blackwell, Oxford. 312 pp.
Taylor, G.H., Teichmüller, M., Davis, A., Diessel, C.F.K., Littke, R., Robert, P., 1998. Organic Petrology. Gebrüder Borntraeger, Berlin. 704 pp.
Varshal, G.M., Velyukhanova, T.K., Chkhetiya, D.N., Kholin, Yu.V., Shumskaya, T.V., Tyutyunnik, O.A., Koshcheeva, I.Ya., Korochantsev, A.V., 2000. Sorption on humic acids as a basis for the mechanism of primary accumulation of gold and platinum group elements in black shales. Lithology and Mineral Resources 35, 538–545.
Vassilev, S., Kitano, K., Vassileva, G., 1996. Some relationships between coal rank chemical and mineral composition. Fuel 75, 1537–1542.
Wan, C., Qiao, X., Yang, J., Kong, H., Zhao, C., 2000. The sporopollen assemblage of the early Cretaceous in Jixi Basin, Heilongjiang Province. In: Zhu, Z., Zheng, G., Zhao, C. (Eds.), Selected Papers of Palynology of Petroliferous Basins. Petroleum Industry Press, Beijing, China, pp. 83–90.
Wang, L.M., 1999. Introduction of the geological feature and explorating of Wulantuga germanium deposit in Xilinguole League, Inner Mongolia. Geology of Inner Mongolia 3, 15–20 (in Chinese with English abstract).
Wang, C., Qian, S., 1981. Early Cretaceous Sporo-pollen assemblages from Ejinuor Basin, Eastern Inner Mongolia. Oil & Gas Geology 2, 373–381 (in Chinese with English abstract).
Wang, C., Zhang, X., 1985. The age of the Linxi Formation. Oil & Gas Geology 5, 403–407 (in Chinese with English abstract).
Wang, X., Dai, S., Sun, Y., Li, D., Zhang, W., Zhang, Y., Luo, Y., 2011. Modes of occurrence of fluorine in the Late Paleozoic No. 6 coal from the Haerwusu Surface Mine, Inner Mongolia, China. Fuel 90, 248–254.
Ward, C.R., 1991. Mineral matter in low-rank coals and associated strata of the Mae Moh Basin, northern Thailand. International Journal of Coal Geology 17, 69–93.
Ward, C.R., 2001. Mineralogical analysis in hazard assessment. In: Doyle, R., Moloney, J. (Eds.), Geological Hazards—The Impact to Mining. Coalfield Geology Council of New South Wales, Newcastle, Australia, pp. 81–88.
Ward, C.R., 2002. Analysis and significance of mineral matter in coal seams. International Journal of Coal Geology 50, 135–168.
Ward, C.R., Spears, D.A., Booth, C.A., Staton, I., Gurba, L.W., 1999. Mineral matter and trace elements in coals of the Gunnedah Basin, New South Wales, Australia. International Journal of Coal Geology 40, 281–308.
Ward, C.R., Matulis, C.E., Taylor, J.C., Dale, L.S., 2001. Quantification of mineral matter in the Argonne Premium Coals using interactive Rietveld-based X-ray diffraction. International Journal of Coal Geology 46, 67–82.
Wedepohl, K.H., 1995. The composition of the continental crust. Geochim et Cosmochimica Acta 59, 1217–1232.
Yang, X., Li, W., Batten, D.J., 2007. Biostratigraphic and palaeoenvironmental implications of an Early Cretaceous miospore assemblage from the Muling Formation, Jixi Basin, northeast China. Cretaceous Research 28, 339–347.
Yudovich, Ya.E., 2003. Notes on the marginal enrichment of germanium in coal beds. International Journal of Coal Geology 56, 223–232.
Yudovich, Ya.E., Ketris, M.P., 2005a. Arsenic in coal: a review. International Journal of Coal Geology 61, 141–196.
Yudovich, Ya.E., Ketris, M.P., 2005b. Mercury in coal: a review. Part 1. Geochemistry. International Journal of Coal Geology 62, 107–134.
Zhang, J., Ren, D., Zheng, C., Zeng, R., Chou, C.-L., Liu, J., 2002. Trace element abundances in major minerals of Late Permian coals from southwestern Guizhou Province, China. International Journal of Coal Geology 53, 55–64.
Zhao, F., Ren, D., Zheng, B., Hu, T., Liu, T., 1998. Modes of occurrence of arsenic in high-arsenic coal by extended X-ray absorption fine structure spectroscopy. Chinese Science Bulletin 43, 1660–1663.
Zhuang, H., Lu, J., Fu, J., Liu, J., 1998. Lincang superlarge germanium deposit in Yunnan province, China: sedimentation, diagenesis, hydrothermal process and mineralization. Journal of China University of Geosciences 9, 129–136.
Zhuang, X., Querol, X., Alastuey, A., Juan, R., Plana, F., Lopez-Soler, A., Du, G., Martynov, V.V., 2006. Geochemistry and mineralogy of the Cretaceous Wulantuga high-germanium coal deposit in Shengli coal field, Inner Mongolia, Northeastern China. International Journal of Coal Geology 66, 119–136.
Zhuang, X., Querol, X., Alastuey, A., Plana, F., Moreno, N., Andrés, J.M., Wang, J., 2007. Mineralogy and geochemistry of the coals from the Chongqing and Southeast Hubei coal mining districts, South China. International Journal of Coal Geology 71, 263–275.
Zilbermints, V.A., Rusanov, A.K., Kosrykin, V.M., 1936. On the question of Ge-presence in fossil coals. Acad. V.I.Vernadsky—k 50-letiyu nauchnoi deyatel'nosti [up to 50-anniversary of his science activity], vol. 1. AN SSSR [Acad. Sci. USSR], Moscow, pp. 169–190.